(2)

OFFICE OF NAVAL RESEARCH

Contract No. N00014-91-J-1409

Technical Report No. 137

IN-SITU ELECTROCHEMICAL SURFACE SCIENCE

by

Michael J. Weaver and Xiaoping Gao

Prepared for Publication

in

Annual Review of Physical Chemistry

Department of Chemistry

Purdue University

West Lafayette, IN 47907-1393

April 1993

INTRODUCTION

The study of electrochemical interfaces is a pursuit almost as diverse as it is venerable. The characterization of such systems, especially for metals in contact with electrolyte solutions, was originally undertaken as a central part of classical physical chemistry during the early decades of this century. More recently, surface electrochemistry has evolved in several different (and somewhat disparate) directions, triggered in part by the wide utility of electrodes in analytical chemistry; indeed, research work along such electroanalytical lines has been emphasized, notably in the USA. The importance of electrochemical interfaces in a variety of technologically important circumstances, including energy conversion and metal corrosion, fuels further our scientific desire to develop a more fundamental physical understanding of the structural and dynamical properties of metal-solution interfaces. The broadbased impact of surface electrochemistry is founded in the unique and controllable interplay between electrical and chemical phenomena afforded at metal-solution interfaces. Thus the continuous alterations in electron energy that can be induced externally at electrochemical interfaces allow subtle (as well as substantial) modifications to the electronic state of interfacial components. One can therefore be justified in asserting that interfacial electrochemistry should form a centrally important part of contemporary surface physical chemistry.

Given the versatile properties of electrode surfaces as redox reagents in solution-phase chemistry, there has long been substantial interest in characterizing as well as manipulating the kinetics and mechanisms of electron-transfer processes at metal-solution interfaces. Such endeavors have been facilitated by the evolution of a battery of electrochemical perturbation techniques based on faradaic current-time measurements, and encouraged by the considerable experimental and theoretical progress made in our understanding of the dynamical and

energetic aspects of solution-phase electron transfers. These efforts have yielded a commonality of understanding between electrochemical and homogeneous-phase redox processes[1,2]. Many important electrochemical redox processes, however, involve chemisorption of the reactant, intermediate(s) and product species, so that the rates and mechanisms are sensitive to the chemical structural nature of the interface. Elucidating the structure of electrochemical surfaces is therefore not only of fundamental significance in its own right, but also is of critical importance for unraveling such interfacial kinetic phenomena.

Most of our knowledge concerning such structural as well as kinetic properties of electrochemical interfaces has arisen historically from measurements of faradaic and/or nonfaradaic currents as a function of electrode potential and/or time[3]. A remarkably diverse body of information continues to be produced from such conventional electrochemical data. The limitation of these measurements, however, lies in their inherently macroscopic nature. As a consequence, our perception of the molecular- and atomic-level structure of electrochemical interfaces has been based more on indirect inference than from direct observation.

In contrast, research within the fundamentally allied subject of metal surfaces in ultrahigh vacuum (uhv)- based environments has long benefited centrally from the availability of a variety of techniques that can yield such microscopic structural information in a relatively direct fashion. This advantageous situation arises from the applicability of electron- as well as photon-based spectroscopies as probes of the electronic and vibrational state of adsorbates, together with the surface structural information afforded by electron, X-ray, and particle diffraction. These factors, along with the ease of preparing as well as characterizing clean ordered single-crystal surfaces in uhv, have over the last 25 years or so spawned the voluminous research area

commonly (if cryptically) termed "surface science", incorporating the chemistry and physics of metal-vacuum interfaces[4].

Despite the close physical relationship between metal surfaces in uhv and electrochemical environments, then, these two research areas have developed along markedly disparate avenues. Within the last 10-15 years, however, there has been substantial progress made in adapting the techniques established in uhv surface science to the microscopic-level characterization of solid metal electrodes. Broadly speaking, such strategies can be divided into three categories. The first group, which are commonly labeled "ex-situ" approaches, involve transfer of the metal surface from the electrochemical cell into a vacuum chamber, with subsequent characterization by uhv-based approaches before possible return transfer and further electrochemical scrutiny [5,6]. This tactic has the obvious virtue of enabling the structure and composition of electrode surfaces to be examined in principle by the full range of "surface science" techniques in addition to separate characterization by electrochemical methods. A central limitation, however, is that the transfer of an intact electrochemical interface into uhv is fraught not only with technical difficulties, but also the solvent and some other interfacial components commonly evaporate into uhv at ambient temperatures.

The alternative vacuum-based approach entails dosing various components of electrochemical interfaces from the gas phase onto a metal surface held at a sufficiently low temperature in uhv. This "non-situ" approach[1], commonly termed "uhv electrochemical modeling", enables ionic as well as neutral interfacial components to be dosed sequentially by employing appropriate ionizable and dipolar species, respectively, enabling their mutual influence to be explored by

---

[1] This terminology was suggested, perhaps wryly, by Eric Stuve.

means of uhv-based techniques[7-9]. While complete electrochemical interfaces ("double layers") can be synthesized and scrutinized in detail, the low temperatures ($\lesssim$ 170K) that are commonly required to avoid interfacial solvent evaporation may jeopardize the connection between such metal-vacuum interfaces and actual electrochemical systems[9].

Consequently, while such "ex-situ" and "non-situ" approaches offer powerful advantages afforded by the availability of uhv-based techniques, the development of molecular-/atomic-level characterization techniques applicable directly to electrochemical interfaces under potential control is clearly of paramount importance. Such "in-situ" methods necessarily have to contend with interferences arising from the presence of the bulk solution. While limiting their scope in comparison with uhv-based methods, a number of in-situ strategies have been developed recently. These are enabling a rapidly expanding array of atomic-/molecular-level information to be obtained for some electrochemical interfaces with a degree of detail and sophistication that is often comparable to that achieved for metal-uhv systems. Encouraging as well as accompanying these developments has been the emergence of reliable procedures for preparing ordered monocrystalline metal surfaces suitable for use in ambient laboratory environments, without recourse to uhv technology. A seminal advance was the demonstration by Clavilier et al that low-index platinum faces could be prepared in a clean ordered state by annealing an appropriately oriented crystal in a air-hydrogen flame, followed by cooling in water and rapid transfer to the electrochemical cell[10,11]. Although initially controversial, this and related methods[12,13] provide now well-accepted means[14] of preparing ordered metal surfaces for in-situ electrochemical purposes.

The primary intent of this chapter is to evaluate some of the notable recent developments in our experimental and conceptual understanding of the

structural properties of metal-electrolyte interfaces that have resulted from these in-situ microscopic-level approaches, especially to ordered monocrystalline surfaces. While emphasis is placed here on the physico-chemical insight that can be deduced from such measurements, the nature of the techniques and their likely spheres of applicability are briefly considered. Also of interest is the possible connection between the properties of metal-adsorbate interfaces so deduced from microscopic-level measurements in corresponding electrochemical and uhv environments. Taken together, the increasing availability of such detailed as well as diverse microscopic-level information for metal-electrolyte interfaces can be considered to constitute the emergence of *in-situ electrochemical surface science*. While the objectives of this research topic have much in common with "conventional" (i.e. uhv) surface science, an intriguing additional theme in electrochemistry involves elucidating the role of the electrical variable (electrode potential or charge) on the structural and dynamical properties of the interface. As already mentioned, remarkable insight into the structural nature of electrochemical interfaces can be obtained from potential-current-time data. The development of in-situ microscopic-level techniques offers intriguing opportunities for their *coupled* application with such conventional electrochemical measurements. Some virtues of this combined approach will be apparent in the illustrative examples discussed below.

We consider here recent experimental findings taken primarily from three types of microscopic-level techniques which can yield direct structural information for both in-situ electrochemical and uhv-based surfaces. The first type, scanning probe microscopies, and in particular scanning tunneling microscopy (STM), has recently been shown to reveal remarkably detailed information on real-space atomic arrangements as well as larger-scale morphologies on ordered metal surfaces in solution as well as in uhv and gas-

phase environments. The second class, X-ray sychrotron-based scattering techniques, provides accurate spatial structural information. Together, these methods are beginning to revolutionize our appreciation of surface crystallography at in-situ electrochemical interfaces. The third category considered here, albeit more cursorily, is surface vibrational spectroscopy, specifically infrared reflection-absorption (IRAS) and surface-enhanced Raman (SERS) spectroscopies. While quite different in character and applicability, both these vibrational techniques can yield important insight into the chemical nature and bonding properties of electrochemical adsorbates, and the influences exerted by the local electrostatic and chemical environment.

The basic properties of these methods for in-situ electrochemical purposes are considered briefly in the following section. Several other in-situ approaches have been developed recently that also can provide additional information on the structure and bonding properties of metal-electrolyte interfaces. The most useful of these in the present context are also noted where appropriate. However, due to restrictions of space (and the personal bias of the authors!), the presentation is decidedly selective. We nevertheless hope that it imparts to the reader at least a flavor of the notable recent progress, current issues and problems, as well as some future prospects in this rapidly evolving research area.

SOME CONTEMPORARY ISSUES AND OPPORTUNITIES

Metal-electrolyte interfaces clearly differ from their metal-uhv counterparts in that solvent and ionic components, along with excess electronic charge, are present in addition to any adsorbed solutes of interest, such as electrochemical reactants. While in a sense rendering the system more complex, these dipolar and "free-charge" solution-phase components, together with the

adjustable electronic charge on the metal surface (collectively, the so-called "double layer"), enable the metal-solution potential drop, ϕ_s^M, to be altered externally in a continuous fashion (vide infra). This property is, of course, central to the practical usefulness as well as the fundamental significance of electrochemical interfaces. With the increasing emergence of in-situ microscopic-level information, it is therefore of central interest to explore the manner in which the structural, electronic, and bonding properties of metal interfaces are dependent upon the external electrical variable. Coupling such potential-dependent microscopic information with the corresponding electrical responses provided by electrochemical measurements offers substantial new opportunities for exploring the interrelationships between surface structure and electronic charge. In addition to establishing links with the behavior of corresponding metal-uhv systems, the electrochemical systems can therefore provide unique insight into electronic factors in surface science.

Several broadbased questions, involving an unorthodox synthesis of notions extant in traditional surface electrochemistry and uhv surface science, suggest themselves which together may be considered to constitute some basic objectives in electrochemical surface science:

(a) Do the metal surface atomic arrangements for monocrystalline electrodes differ from the bulk termination structure (i.e. does surface reconstruction occur)? How do the structures depend on the surface potential and the occurrence of chemisorption?

(b) How do these structures compare, and relate, to metal surface reconstruction in uhv?

(c) How is the surface mobility of substrate metal atoms dependent on the electrode potential and interfacial composition?

(d) What is the nature, and conditions of occurrence, of ordered interfacial

structures for adsorbed solutes, electrolyte ions and solvent molecules?

(e) What is the origin(s) of the influence of the electrical variable (metal electronic charge or surface potential) upon metal-adsorbate bonding?

(f) How, and in what manner, can one distinguish between specific and nonspecific double-layer effects upon adsorbate structure and bonding?

(g) In what fashion can one interrelate the potential-dependent structural and bonding properties of electrochemical interfaces with those for corresponding metal surfaces in uhv?

(h) How can one connect the structural and bonding properties of monocrystalline electrochemical interfaces with their catalytic activity, i.e. the rates of inner-sphere and other catalyzed electron-transfer reactions?

We outline below some recent findings from in-situ experiments that at least in optimal cases provide significant new insight along these lines. It is appropriate beforehand to comment briefly on the nature of the in-situ techniques being utilized for this purpose.

NATURE OF IN-SITU PROBES IN SURFACE ELECTROCHEMISTRY

As already alluded to, a major impediment to the application of spectroscopic and other microscopic-level techniques to in-situ electrochemical interfaces lies in the need for the probe and resultant signal to traverse at least one of the adjacent bulk phases, usually the electrolyte solution. The adaption of methods utilized in uhv surface science therefore commonly needs to contend with bulk-phase solution interferences, which can often obscure entirely the sought-after component of the signal associated with interfacial phenomena. There are two distinct circumstances, however, under which one can extract the latter desired signal with suitably high sensitivity. The first involves methods for which the interface provides the sole (or at least preeminent) contribution

to the measured signal, so that bulk-phase interferences are necessarily absent except for possible interactions with the incoming probe (and/or the outgoing signal). Methods exhibiting these characteristics can be categorized as "intrinsic surface-sensitive" techniques. Important examples include surface-enhanced Raman scattering (SERS), second harmonic generation (SHG), and scanning tunneling microscopy (STM) (vide infra).

For the majority of techniques desired to be employed for in-situ electrochemical purposes, however, the signal resulting from interfacial species, for example for infrared absorption spectroscopy, does not differ greatly in kind from that associated with corresponding bulk phase components. In this circumstance, the much larger number of bulk-phase relative to interfacial species present will usually result in spectral responses that arise predominantly from the former rather than the latter. Nevertheless, the deleterious influence of the former component can be minimized and even essentially eliminated in several ways.

Most commonly, the photon path length through the solution is diminished dramatically by employing thin-layer optical configurations[15]. These planar geometries, most straightforwardly accomplished by pressing together the electrode surface and a flat optical window, typically yield solution thicknesses of the order of 2-10 μm. This cell arrangement offers the important virtue of being largely transparent to photons over a wide wavelength range, even for large segments of the infrared region. Moreover, for strongly adsorbed solute species (i.e. those where only low solution-phase concentrations are required), thin-layer cells can yield quantities of adsorbate in the reflected optical path that are comparable to the corresponding solution species, thereby aiding detection of the former in the face of the latter. Another tactic, most commonly employed in conjunction with infrared reflection-absorption spectroscopic (IRAS)

measurements, involves acquiring difference spectra between a pair (or sequence) of electrode potentials. The virtue of this procedure is that it selectively recovers *potential-dependent* spectral components, often arising from interfacial species, even in the face of markedly larger yet potential-independent interferences, most prominently from the bulk-phase solvent.

Microscopic-level methods that do not offer intrinsic surface sensitivity, but can be induced to do so when employed in conjunction with such tactics can be labeled as "extrinsic surface-sensitive" techniques. Key examples include the various forms of potential-difference infrared spectroscopies, X-ray diffraction, X-ray absorption spectroscopy, and radioactive labeling methods.

Some further comments are in order regarding the pair of in-situ approaches that are emphasized here. Scanning tunneling microscopy undoubtedly constitutes the most remarkable development in surface science techniques over the last decade[16,17]. While the key demonstration that true atomic-resolution images can be observed for ordered metal surfaces in uhv was achieved early in the development of STM, corresponding atomic-level applications to in-situ metal-solution interfaces are of much more recent origin[18,19]. Nevertheless, STM is extremely well suited to the in-situ characterization of metal-electrolyte interfaces. The occurrence of stray faradaic currents involving the STM tip can be essentially eliminated by insulating the wire, so that the measured surface-tip currents arise exclusively via elastic tunneling even in the presence of substantial faradaic electrochemistry at the substrate-solution interface[20]. Consequently, then, STM constitutes an "intrinsic surface-sensitive" in-situ technique by the above definition, providing a powerful means of elucidating real-space atomic-level (and also larger-scale) structure for ordered electrode surfaces under potential control.

It is nonetheless worth mentioning that some differences in the nature of

the tip-substrate electron-tunneling process between corresponding uhv and electrochemical environments might be anticipated, based on the possible involvement of intervening solvent or other species. So far, information on the detailed nature of metal-metal electron tunneling STM for both interfacial environments is rather sketchy, especially at the atomic level, due in part to the difficulty of obtaining sufficiently reproducible (and stable) current-bias voltage and related data under systematically varying conditions. Nevertheless, the similarly detailed form of the STM images obtained, for example, on monocrystalline gold surfaces in uhv and solution-phase environments suggests that the aqueous solvent exerts relatively little effect upon the tunneling physics. This general observation is consistent with the likely small (< 5-10 Å) tip-substrate distances probably required in order to obtain atomic-resolution STM images, given that water is known from molecular electron-transfer studies not to facilitate electron transmission between redox centers.

Concurrently with the development of STM, synchrotron-based X-ray techniques have emerged as another powerful means of securing in-situ information on spatial atomic structure at ordered metal-solution interfaces[21]. In particular, grazing-incidence X-ray scattering (GIXS) can yield extremely accurate crystallographic parameters for both the metal substrate and suitable adlayers[21a]. The key elements favoring such in-situ applications of X-ray based techniques are the considerable penetration depth of hard X-rays into water (and other solvents), along with the availability of sufficient beam intensity from synchrotron sources to engender measurable diffraction, etc., from the surface region[21a]. We now consider recent illustrative examples of the application of both in-situ STM and GIXS to the elucidation of ordered metal surface and adlayer atomic arrangements. Given the very different physical basis of these techniques, along with their inherently complementary nature, the

intercomparison of structural data extracted for the same (or similar) systems is of obvious interest.

ELECTROCHEMICAL SURFACE CRYSTALLOGRAPHY

Perhaps the most important current issue in electrochemical surface science concerns the elucidation of the spatial atomic arrangements of the metal substrate atoms, together with any ordered atomic or molecular adlayers present. While this topic is of course common to metal surfaces in vacuum as well as electrochemical environments, an intriguing additional theme in the latter case concerns the role of the electrical variable in triggering phase transitions and other alterations in interfacial structure. Beyond the general issues (a)-(d) noted above, a number of specific questions, precipitated in part from analogous considerations for metal-uhv interfaces, arise in this context: Do the surface metal atoms exhibit long-range order? What is the atomic arrangement (unit cell, etc.) of the top-layer metal atoms, and its long-range structural propagation? How does the surface atomic structure depend on the electrode potential (or surface electronic charge)? For potential-dependent adsorption (especially for anions, metal cations), at what coverages do ordered adlayers form? What is the dependence of the adlayer symmetry upon coverage? What are the adsorbate-surface binding sites?

Until very recently, most information relating to these questions was extracted from ex-situ experiments utilizing uhv electron-diffraction techniques[22]. Over the last 2-3 years, however, a significant number of STM and GIXS studies have been reported which demonstrate the remarkably detailed insight that can be obtained by direct in-situ measurements under electrode-potential control. To illustrate these points, we now consider some selected examples.

Potential-Dependent Surface Reconstruction

Gold surfaces occupy a special position in electrochemistry in view of their unique resistance to oxidation and the availability of wide polarizable potential ranges even in aqueous media. The seminal work of Hamelin and coworkers established protocols for preparing and characterizing monocrystalline gold, as well as silver, electrodes in aqueous solution, and mapped out their electrochemical behavior[13]. On the basis of observed hysteresis in capacitance-potential (C-E) and cyclic voltammetric (current-potential) behavior, it was suggested that gold low-index surfaces undergo reconstruction at negative electrode charges[23]. Indeed, all three low-index gold surfaces are known to reconstruct spontaneously in uhv[24]. Detailed and elegant support for the occurrence of negative charge-induced surface reconstruction of these gold surfaces in aqueous solution, along with removal ("lifting") of the reconstruction at positive electrode charges, was obtained by Kolb and coworkers on the basis of ex-situ electron-diffraction measurements, as well as by in-situ uv/visible electroreflectance spectra and C-E data[22b,25]. These findings were also corroborated by in-situ SHG measurements for Au(100)[26] and Au(111)[27] by exploiting the changes in SHG rotational anisotropy engendered by the alterations in net surface symmetry occurring upon reconstruction.

In-situ GIXS data have recently been reported for all three low-index gold electrodes[28-30]. The diffraction patterns for Au(100) in aqueous perchloric acid clearly indicate the occurrence of a near-hexagonal reconstructed overlayer of gold atoms rotated slightly (0.8°) from the [110] axis, which forms slowly ($\gtrsim$ few minutes) at small negative electrode charges[28a]. For Au(110) in halide electrolytes, (1 × 3) missing-row reconstructions are seen to be formed rapidly under these conditions[30].

Monocrystalline gold electrodes, especially Au(111), have been the focus

of STM studies emanating recently from several laboratories. This emphasis reflects not only their desirable electrochemical properties, but also the relative ease by which gold can withstand the rigors of electrode transfer and assembly of the in-situ STM cell without serious surface contamination. Indeed, gold electrodes were featured in some of the first reports of atomic-resolution STM images for in-situ electrochemical cells[18]. In our laboratory, we have recently examined by in-situ STM the potential-dependent surface atomic structures for a number of monocrystalline gold faces, including the three low-index planes[31-34]. Related in-situ studies have been reported by other groups[35-37].

Besides confirming the occurrence of reconstruction of each low-index face at negative electrode charges in the absence of ionic adsorption, which is lifted at positive charges, the STM data provide some intriguing structural and dynamical details. Figure 1 shows an atomic-resolution STM image obtained for Au(100) in aqueous 0.1 M $HClO_4$, taken from ref. 32b. The initially unreconstructed surface[32c] was adjusted to an electrode potential (-0.3 V vs saturated calomel electrode, SCE), corresponding to a small negative electronic charge density, 2 minutes before this image was recorded (see ref. 32b for details). The right-hand central portion of the image in Figure 1 displays a square planar array of sharp tunneling maxima spaced 2.9Å apart, consistent with a (1 × 1) (i.e. unreconstructed) array of gold surface atoms. Evident in the left-hand portion of the image, however, is a radically different structure, consisting of near-hexagonal atomic packing. The observed "string-like" atomic pattern displays distinct z-corrugations in both directions of the unit cell. (This structure is seen in successive images eventually to encompass almost the entire imaged area.) Intercomparisons of the two adjacent [reconstructed, (1 × 1)] domains yields detailed information on the nature of the reconstruction.

Briefly, a (5 × 27) unit cell can be deduced directly from the real-space periodicity of the z-corrugations[23b], closely similar to the structure deduced for clean reconstructed Au(100) in uhv from low-energy electron diffraction (LEED)[38]. Furthermore, examination of larger-scale STM images demonstrates that the reconstruction can propagate so to form a variety of long-range superstructures, yielding in particular subtle variations along the long unit-cell direction so to circumnavigate terrace edges and other surface defects[23b]. This flexibility of the top layer-substrate registry is apparently unique to Au(100) and (111); it probably reflects the prevailing influence of bonding between top-layer atoms relative to interactions with the underlying substrate.

The reconstructed domains on Au(100) are seen to appear only slowly in perchlorate and other weakly adsorbing electrolytes, requiring ca 10–15 min for extensive potential-induced formation. The reconstruction dynamics are expected to be controlled in part by the surface mass transfer of gold atoms, given that the (5 × 27) phase has a 24% higher surface atomic density than for the (1 × 1) interfaces. The STM probe provides a valuable means of following the changes in surface morphology over a range of distance scales accompanying such phase transformations, therefore lending insight into the real-space dynamics that are involved.

A simple example of the application of STM for this purpose is shown in Figure 2A and B. The latter STM image, for Au(100) in aqueous 0.1 M H_2SO_4, was obtained while the substrate electrode potential was swept linearly at 10 mV s^{-1} from 0.3 V to 0.5 V vs SCE. The image was acquired over ca 20 s by rastering the tip gradually downward; consequently the y-axis can be considered to be a potential/time scale (increasing from top to bottom) as well as the real-space axis as marked. The top half of the image (corresponding to E = 0.3 to 0.4 V) displays three "ribbon-like" features, characteristic of (5 × 27) reconstructed

domains. (These were formed by holding the potential at −0.4 V beforehand.) In the preceding image (corresponding to E = 0.1 to 0.3 V) shown in Figure 2A, these ribbons extend uniformly from top to bottom of this surface region. However, Figure 2B shows that the reconstruction is removed abruptly in the middle of the image, corresponding to the potential being swept positive of ca 0.4 V, being replaced by several large (4–8 nm diameter) gold clusters[32d].

The sharp lifting of the Au(100) reconstruction under these conditions has been described elegantly by Kolb et al on the basis of electrochemical and in-situ electroreflectance measurements[25]. In particular, a sharp current-potential peak is obtained in the positive-going potential scan of the cyclic voltammograms, which coincides with the potential at which the reconstruction is lifted[25a]. This spike arises from the need to remove electronic charge from the metal surface when the (1 × 1) phase is formed, associated in part with the lower potential of zero charge, E_{pzc}, for this structure compared with the hexagonal reconstructed surface phase[25a]. (We consider another example of this electrochemical phenomenon below.) The STM data, however, reveal valuable additional information concerning the spatial rearrangements that accompany (and indeed are responsible for) this fundamental surface phase transformation. Such real-time/real-space STM data also yield some insight into the observed sensitivity of the surface reconstruction to the electrolyte anion[32d]. Thus sequencies of STM images acquired during appropriate potential steps or sweeps show how the surface mobility of gold atoms, and consequently the dynamics of forming as well as lifting the reconstruction, is accelerated greatly by anion adsorption. Particularly in iodide electrolytes, the Au(100) reconstruction dynamics become largely reversible as well as extremely rapid; this potential-induced phase transition is seen by in-situ STM to be accompanied by collective surface migration of gold atoms over remarkably large distances, ca 10–50 nm,

within a few seconds. Evidently, the occurrence of strong anion-metal bonding not only aids the equilibrium removal of surface reconstruction, but also facilitates greatly the large-scale surface transport of metal atoms required for this phase transition to occur[32d].

It is worth mentioning that the interfacial forces responsible for the potential-dependent stability of the surface reconstructions seen for monocrystalline gold surfaces are not well understood at present[39]. Given that elevated temperatures are usually required to engender such phase transitions on metal surfaces in uhv, it is noteworthy that only small electronic charge densities (typically $\lesssim 0.05$ e^- per surface metal atom) can readily trigger the formation and removal of surface reconstructions at gold-aqueous interfaces. Indeed, structurally dramatic "missing-row" reconstructions on Au(110) can form very rapidly ($\lesssim 1$ s) even in aqueous perchlorate media[33]. Theoretical efforts aimed at acquiring at least a qualitative conceptual understanding of potential-induced reconstruction are starting to appear[40]. It will be of interest to ascertain if this phenomenon can be observed for other metal-solution interfaces, especially for platinum-group transition metals.

Potential-Dependent Adlayer Structures

Besides the structure of the metal substrate itself, elucidating the nature and extent to which chemisorbates form ordered atomic/molecular arrangements is clearly of central interest. In the same vein as for metal reconstruction, much information on the nature of ordered atomic and molecular adlayers at metal-uhv interfaces has been obtained from LEED measurements[24]. This technique has also proved useful for deciphering electrochemical adlayer structures in some cases by using ex-situ tactics[5,6]. As for substrate reconstruction, detailed in-situ diffraction information for such electrochemical adlayers are beginning to be

obtained by GIXS[21].

While systematic studies are lacking so far, STM measurements of adlayers on metal surfaces in uhv and also gas-phase (including air) environments are now sufficiently widespread to demonstrate the power and versatility of the technique for this purpose[41]. Such observations bode well for the future of related applications at in-situ electrochemical surfaces. We briefly outline here some applications along these lines, specifically to the potential-dependent adsorption of anions and upd (underpotential deposited) metals. The examples are chosen in part to illustrate the value of *combined* electrochemical and STM data, and the complementary nature of in-situ GIXS and STM measurements for adlayer characterization.

Of the various anionic adsorbates of common electrochemical significance, iodide is particularly amenable to examination by both STM and GIXS. Thus iodide binds strongly to a number of solid metal electrodes, notably platinum and gold, in largely covalent fashion (i.e. forming essentially uncharged iodine adatoms). Schardt and coworkers first demonstrated the suitability of STM for obtaining detailed structural information for iodide adlayers on Pt(111)[19,42]. The high atomic mass of iodine also facilitates its detection in X-ray scattering. The examination of iodide adsorption on gold electrodes by electrochemical as well as microscopic techniques is aided by the wide polarizable potential range available, enabling the adsorbate coverage to be varied from near-zero to saturated values for a given solution iodide concentration merely by increasing the electrode potential. This marked sensitivity of the adsorption thermodynamics to the electrode potential is a hallmark of ionic adsorbates, especially those featuring charge transfer upon adsorption. (Indeed, the electrode potential can usefully be conceived as being equivalent to a logarithmic scale of iodine "chemical potential," or pressure, as would be encountered in the

analogous gas-phase adsorption system.) We have recently explored the potential-dependent adlayer structures of iodide on low-index gold-aqueous interfaces by means of in-situ STM along with electrochemical measurements[43-45]. In addition, Ocko and coworkers have undertaken in-situ GIXS measurements for these systems under similar conditions[46].

We will now consider the Au(111)-I^- system as an instructive example of the combined value of such electrochemical/STM/GIXS measurements, with additional comments for Au(110) and Au(100). Figure 3 shows a cyclic voltammogram obtained for Au(111) in aqueous 0.1 M $NaClO_4$ containing 5 mM NaI. The sweep rate is 50 mV s^{-1}. Over the potential range selected, -0.7 to 0.3 V vs SCE, faradaic electrochemical processes are absent (i.e. no redox transformations occur, save for the partial adsorbate-metal charge transfer attending iodide adsorption). Instead, the observed current-potential features reflect largely the occurrence of potential-dependent iodide adsorption, perhaps coupled with cation adsorption[47]. Most prominently, large current-potential (i-E) maxima are observed during both the positive- and negative-going potential sweeps, labeled A and A', respectively. These features arise from the adsorption (and desorption) of iodide. The magnitude of the capacitive current will be roughly proportional to $d\theta_I/dE$, where θ_I is the iodide coverage. (Physically, the current can be considered to arise from the electron flow associated with the positive "surface image charge" formed upon iodide adsorption, together with the partial adsorbate-surface charge transfer.) On this basis, iodide adsorption commences at about -0.7 V, and would appear to approach near-saturation coverages by about -0.25 V. (Indeed, adsorbate surface concentrations can be deduced directly from related differential capacitance - E data, obtained most conveniently from ac impedance measurements[49].

Provided that the potential-dependent adsorption/desorption process is

entirely reversible, the positive- and negative-going voltammetric sweeps will form mirror images. Careful inspection of Figure 3 shows that this is only partly the case. In particular, the sharp peak B is only evident during the positive-going potential sweep, and the smaller feature D/D' exhibits some hysteresis.

Examination of in-situ atomic-resolution STM data, especially that acquired during related potential excursions, allow these electrochemical responses to be matched with specific surface structural transformations. At the most negative potentials, atomic-resolution STM images indicate the presence of a uniformly ($\sqrt{3}$ × 22) reconstructed surface[31]. This pattern gives way to a (1 × 1) hexagonal structure when the potential is swept just beyond peak B, showing that there is sufficient iodide adsorption to lift the reconstruction at this point[45]. Throughout the potential region ca −0.6 to −0.3 V, corresponding to extensive iodide adsorption on the basis of Figure 3, the STM images exhibit only substrate atomic patterns, suggesting that the iodide adlayer is disordered and/or mobile under these conditions.

When the potential is shifted positive of the reversible voltammetric peak C (Figure 3), the STM images exhibit iodide adlayer patterns. An example of this potential-induced structural ordering is shown in Figure 4A, obtained for Au(111) in 0.1 M $HClO_4$ + 0.5 mM KI[43]. The lower portion of this STM image was obtained at −0.4 V vs SCE, the potential being stepped to 0.1 V about halfway along the upward-rastered STM scan. The bottom half of this dual (or "composite-domain") image shows the hexagonal (1 × 1) pattern characteristic of the unreconstructed substrate. The upper portion, however, exhibits a markedly different quasi-hexagonal pattern, similar to the ($\sqrt{3}$ × $\sqrt{3}$)R30° structure (θ_I = 0.33) commonly observed for atomic adsorbates on (111) surfaces in uhv[24]. Close inspection of the STM patterns reveals a significant departure from this pattern, featuring

a pair of iodine row directions shifted by a few degrees from the R30° direction, with a resultant compression of the I–I distance, yielding an approximate (5 × $\sqrt{3}$) (θ_I = 0.4) unit cell. (While such subtle differences in real-space adlayer structure are not readily discerned from absolute STM images given the x-y distortions commonly arising from piezo drift, they can be detected readily in dual images such as Figure 4A by employing the substrate pattern as an "internal calibration"[43].) Similar (5 × $\sqrt{3}$) patterns have been observed for the Au(111)–I system by LEED following electrode emersion[47] and by high-precision STM in air[48].

The occurrence of such ordered Au(111)–I structures in this potential region has also been deduced from in-situ GIXS measurements by Ocko et al[46]. Significantly, the extremely high accuracy of GIXS has also clearly identified the presence of a *continuous* variation in adlayer symmetries over the potential range ca −0.3 to 0.15 V, featuring a gradual uniaxial compression of a pair of I rows away from the hexagonal ($\sqrt{3}$ × $\sqrt{3}$) (θ_I = 0.33) structure towards (and beyond) the (5 × $\sqrt{3}$) pattern (θ_I = 0.4). This phenomenon has been confirmed by high-precision STM data[48b]. The STM data show that the iodines remain bound in multifold (bridging/hollow) sites under these conditions[43]. Finally at about 0.15–0.2 V, corresponding to the voltammetric peak D (Figure 3), a more compressed hexagonal adlayer structure ($\theta_I \approx$ 0.43–0.45) is evident from both STM and GIXS[43,48,48]. The STM images display an interesting corrugated pattern, shown in Figure 4B. The undulations in the iodine adatom intensity arise from periodic variations in the binding site from hollow to atop geometries (cf Au(100) reconstruction above), obliged by the near-saturated surface packing. (The I–I distance approaches the van der Waals diameter, 4.3Å.)

Taken together, such potential-dependent structural data provide an intriguing picture of the complex interplay between adsorbate–surface bonding and

steric packing factors that can allow an atomic-level interpretation of the corresponding electrochemical responses, such as in Figure 3. A schematic summary of the potential-dependent findings gathered in this fashion for Au(110)-I in comparison with Au(111)-I is illustrated in Figure 5, in the form of iodine coverage-potential (θ_I - E) profiles, segments being labeled with approximate ball-model structures (as deduced by STM or GIXS) as appropriate. Several significant features are evident from this summary. First, structurally ordered adlayers are formed only at high iodine coverages, within 80-90% of saturation; region I, in which the θ_I - E profiles are extracted from electrochemical data, can therefore be surmised to involve "gas phase-like" adsorption. Note that iodide adsorption on Au(110) commences at markedly more negative potentials than on Au(111). This characteristic difference arises in part from the ca 0.3 V lower E_{pzc} (lower work function), together with the greater coordinative unsaturation, for the former surface. Region II constitutes the emergence of sufficient adsorbate packing to engender a "liquid-crystal" phase, displaying long-range order along with significant compressibility. (Such compressibility can readily be discerned by STM on Au(110), and on Au(100), from the continuous progressive shifts in the periodicity of the z-corrugated structures observed upon altering the electrode potential[45].) On both Au(111) and Au(110), the approach to saturation involves a first-order phase transition to a distinctly different adlayer symmetry, accompanied by a sharp voltammetric spike (such as D in Figure 3). On Au(110), a further "crystalline phase" IV is observed by STM, involving longer-range substrate restructuring[45]. Finally, for $E \geq 0.4V$, I-I surface *bonding* to yield eventually multilayer polyiodide films is discerned, accompanied by the onset of solution-phase iodide electrooxidation[43].

Such potential-dependent STM (and GIXS) findings can therefore now realize the true in-situ equivalent of the elegant ex-situ LEED and related structural

strategies pursued in particular by the Hubbard school[5]. One of the advantages of the in-situ approach is that considerable additional information on the real-space *dynamics* of potential-induced surface structural changes may also be obtained. An example along these lines, for dissipation of the Au(100) reconstruction, has been noted above. A particularly useful tactic involves obtaining parallel (or simultaneous) voltammetric and STM data. The former measurements, with appropriate variations in potential sweep rate, etc., can provide information on the overall phase-transition kinetics. (For example, the hysteresis and peak width of the D/D' i-E feature for Au(111)-I in Figure 3 are both increased markedly towards faster sweep rates.) The STM measurements, however, offer intriguing additional information on the local (down to atomic-level) dynamics, including dependencies on terrace size, the role of defects, and so on. This constitutes an interesting new vista in electrochemical surface science.

Few in-situ atomic-level adlayer structures have been reported so far for other anionic adsorbates. Bromide provides an interesting comparison with iodide since electrochemical thermodynamic measurements show that the former retains a markedly larger fraction of its anionic charge upon adsorption on gold[50]. Nevertheless, the Au(111)/Br^- system yields an approximate ($\sqrt{3} \times \sqrt{3}$) pattern[51] along with a noncommensurate near-saturated structure, also similar to Au(111)/I[52]. An interesting ordered STM pattern for adsorbed bisulfate has been reported at high potentials on Au(111), which is absent on Au(100) and (110)[53]. Its sharp potential-induced appearance coincides with a voltammetric peak, suggestive of an order-disorder transition (cf iodide above).

Particular recent attention has been devoted to the elucidation of upd adlayer structures by in-situ STM, AFM and GIXS methods[18,54-58]. This reflects the substantial electrochemical interest in the upd phenomenon, by which metal

ions can be electroreduced to form uniform submonolayer deposits at electrode potentials that can be substantially less negative than required for multilayer ("bulk-phase") metal deposition[59]. A number of upd adlayer metals (Tl, Pb, Bi, Hg, Ag, Cu) have been the subject of in-situ atomic-level STM, AFM, and GIXS studies, primarily on Au(111) and Ag(111)[18,54-58].

In several cases, for example Cu on Au(111)[18,55a,57,58a] and Ag on Au(111)[55b], ordered upd adlayers are observed by STM and AFM that seemingly correspond to coverages well (> 1.5-2 fold) below the anticipated close-packed limit. Interestingly, the occurrence as well as geometry of these structures is very sensitive to the nature of the supporting electrolyte anion[55,57]. This point has been explored extensively by Gewirth et al using AFM[55]. The results suggest that ordering in such low-coverage upd adlayers is being facilitated by coulombic interactions, with the electrolyte anion being incorporated into the metal atomic lattice. For example, a $(\sqrt{3} \times \sqrt{3})R30°$ adlayer (θ = 0.33) is seen by both STM and AFM for Cu on Au(111) in sulfuric acid electrolyte [55a,57,58a], whereas only a close-packed (1 × 1) adlayer (θ = 1.0) is seen in perchloric acid[55a], inferring that the former structure intimately involves adsorbed SO_4^{2-} (or HSO_4^-) as well as upd copper. The addition of chloride to the former system also affects greatly the copper upd structure[57], which in turn can influence the morphology of subsequent multilayer copper depositions[57b]. The independent examination of these systems by X-ray techniques will be enlightening.

For larger adatoms, such as Tl and Pb, coverages close to the close-packed limit are seen by GIXS to be formed throughout the upd potential region[54], although the possible effects of varying the electrolyte anion have received less attention[54c]. Analogously to the iodine adlayers considered above, these high-coverage upd systems yield complex noncommensurate structures that undergo continuous compression as the electrode potential is altered towards the bulk

deposition value[54]. The virtue of the GIXS technique for obtaining subtle yet significant adlayer structural alterations associated with this compression is well demonstrated in these studies[54]. An illustrative example of the structural insight that can be obtained from such GIXS measurements for upd Bi on Ag(111) is shown in Figure 6, taken from ref. 54f and g. The ball model (A) depicts the adlayer structure deduced in this manner, featuring a fixed $\sqrt{3}$ adlayer spacing in the vertical (a) direction, along with a variable noncommensurate packing along the horizontal (b) axis. Altering the potential towards more negative values yields a continuous increase in Bi coverage achieved purely by a diminution of the interatomic distances in the b direction, as illustrated in Figure 6B. This uniaxial adlayer compression is therefore very similar to that noted above for the Au(111)-I system. Interestingly, upd Tl and Pb layers on Ag(111) undergo *isotropic* compression towards more negative potentials[54]. Evidently, then, the nature as well as occurrence of such potential-induced adlayer compression is sensitive to the physical (and possibly chemical) properties of the upd species.

Despite the extensive attention given to the upd adsorbate systems, there has so far been surprisingly little overlap in the systems examined by the probe microscopy (STM, AFM) and GIXS techniques. An exception is a recent study comparing upd Bi on Au(111) in perchloric acid scrutinized by means of STM, AFM, and GIXS[56]. This system exhibits both low-coverage (2 × 2) (θ = 0.25) and near-saturated (θ ~ 0.6-0.65) adlayer structures, observed by all three techniques. Examples of AFM images obtained for the Au(111) substrate, and the (2 × 2) and high-coverage incommensurate structures for upd Bi, taken from ref. 55d, are shown in Figures 7A-C. As for Ag(111)/Bi (Figure 6), the Au(111)/Bi system exhibits a uniaxial compression at high packing densities. Similarly to the iodine systems, this noncommensurate Au(111)/Bi adlayer yields z-corrugations

("moire pattern") in the STM (but, oddly, not the AFM) images, consistent with periodic variations in the symmetry of the bismuth binding sites along the adlayer row directions[56]. The compressibility of the noncommensurate Au(111)/Bi adlayer, as evaluated by GIXS, is significantly different to that for Ag(111)/Bi[56].

There are few reports so far of the characterization of ordered molecular adlayers on electrode surfaces by these (or other) in-situ techniques. Exceptions include some DNA bases (nitrogen heterocycle) adsorbates on Au(111)[63] and saturated carbon monoxide adlayers on Rh(111) and (110)[64]. (The latter will be considered further below.) This dearth of information reflects in part the emphasis placed so far on gold surfaces, for which chemisorption of organic molecules may commonly be insufficient to yield suitably immobile and ordered adlayers. The typically stronger chemisorption of aromatic molecules on platinum-group transition metals should provide substantial opportunities along these lines. Besides the elucidation of molecular packing arrangements, in-situ probe microscopies can be anticipated to yield considerable insight into adsorbate molecular structure and orientation. The examination of electroactive adsorbates in this regard would be of particular interest.

As for metal surface reconstruction, some insight into the symmetry properties of ordered adlayers can be extracted by SHG rotational anisotropy measurements. Some particularly interesting applications of this tactic to the examination of adlayers on Pt(111) in aqueous perchloric acid have been described by Corn and coworkers[60]. In addition to characterizing the symmetry properties of saturated iodine and carbon monoxide adlayers, the SHG measurements also indicated the presence of an ordered adlayer, most likely adsorbed hydrogen, over a range of potentials below the so-called "butterfly" voltammetric feature[60a]. This supports the original notion that the butterfly feature arises in part from

the oxidative removal of "anomalous" adsorbed hydrogen[10]. The surface structural information provided by in-situ SHG is inevitably less direct and complete than that furnished by probe microscopies and X-ray techniques. These studies nonetheless demonstrate the value of SHG for electrochemical adlayer characterization in that the technique can detect and characterize adlayers such as hydrogen that are difficult or even impossible to examine by in-situ microscopic or diffraction methods.

While this research topic is undergoing rapid development at this writing, it is appropriate to draw on the experimental headway made so far for both anionic and upd systems in commenting on the anticipated development of a more unified understanding of electrochemical adlayer structure. The emphasis so far in STM, and especially GIXS, measurements has been on the elucidation of individual adlayer structures. While such studies are often very elegant and worthwhile in themselves, relatively little attention has been given to examining the manner in which such structural patterns are sensitive to systematic variations in the chemical and stereochemical properties of the adlayer, substrate, and electrolyte species. More methodical studies along these lines are clearly necessary before meaningful broadbased trends concerning electrochemical structures can be enunciated. One central issue concerns understanding the electrostatic influence of the double layer, coupled perhaps with more specific effects from coadsorbed electrolyte ions (vide infra). Interest in such phenomena arises partly from their uniqueness to the electrochemical environment; a greater variety of structural patterns might be anticipated in comparison with related adlayers at metal-uhv interfaces.

As illustrated above, the electrical variable can be utilized in conjunction with STM to gain diverse additional information, such as adsorbate binding sites and the dynamics of adlayer phase transitions. This ability to

alter as well as control the adlayer structure and composition by suitable electrode-potential perturbations in concert with STM measurements is clearly an invaluable tactic from several standpoints. Another promising application of in-situ probe microscopies coupled with electrode-potential perturbations involves the atomic-level characterization of molecular adlayers formed by (or otherwise involved in) electrochemical processes. Examples include a pair of STM studies of electrogenerated iodine and polysulfur films on Au(111)[43,61]. Metal electrodeposition represents a particularly important example in which surface structural changes brought about by faradaic electrochemical events can be scrutinized by means of in-situ STM. Significant issues here include the larger-scale nature of the nucleation-growth process as well as atomic-level adlayer structures[62]. Of paramount interest in all these studies is linking the electrical responses furnished by conventional electrochemical measurements with the potential-dependent structural changes identified by the in-situ microscopic technique. Such combined electrochemical-microscopic tactics clearly provide unique new opportunities for exploring both the structural and dynamical aspects of ordered phases in surface science.

ADSORBATE VIBRATIONS

While the probe microscopy and X-ray techniques can provide detailed insight into the spatial positions of adsorbed atoms and molecules, a more complete assessment of surface bonding requires in particular information on the adsorbate vibrational properties. As already noted, both IRAS and SERS have been applied extensively to the in-situ vibrational characterization of adsorbed species at metal-solution interfaces[65,66]. The strengths and weaknesses of these two methods are markedly different, especially for electrochemical applications. Infrared spectroscopy offers the advantages of clearcut surface

selection rules and applicability to a variety of surfaces, including oriented single crystals. On the other hand, the useful frequency range is fairly restricted, being limited chiefly to the "mid-infrared" region. In contrast, SERS offers intrinsic surface sensitivity, and can readily yield vibrational spectra over wide frequency ranges, including the region below ca 700 cm^{-1} where surface-adsorbate vibrations are commonly located. The major limitation of SERS, however, lies in the need for surface roughening to induce the Raman enhancement, which largely eliminates the use of oriented single crystals, along with its practical restriction to silver, copper, or gold substrates. This last difficulty, in particular, has limited the range of surface electrochemical applications of SERS, the technique can be extended to a range of other surface materials, including transition metals, by depositing them as ultrathin films on a suitable SERS-active template[74].

Together, then, IRAS and SERS form a complementary pair of in-situ vibrational spectroscopic techniques that have already yielded a wealth of information for both stable and reactive adsorbates at metal-solution interfaces. Various aspects of the electrochemical applications of IRAS[15,65,67] and SERS[66] have been reviewed in detail recently. As a consequence, we restrict our attention here to a brief consideration of some findings regarding surface potential- (and charge-) dependent adlayer bonding that are pertinent to the foregoing discussion.

Influence of Electrical Variable on Adlayer Bonding

Carbon monoxide has long been considered to be the archetypical simple molecular chemisorbate in electrochemical as well as uhv surface science. Its significance in the former area stems in part from the common presence of CO as a chemisorbed poison during electrocatalytic organic oxidations[68]. More

generally, adsorbed CO is of interest in view of its ready detection by infrared spectroscopy, and the sensitivity of the C–O stretching frequency, ν_{CO}, to the surface coordination geometry and local environment. In view of the extensive detailed vibrational information available for CO adlayers on ordered metal surfaces in uhv, the comparison between the spectral properties within corresponding electrochemical and uhv environments should yield substantial insight into the likely roles of the electrical double layer.

Some detailed investigations along these lines have been pursued recently in our laboratory (for overviews, see refs. 64b, 67, 69). Figure 8 shows illustrative infrared spectra obtained in the ν_{CO} region for CO adlayers dosed on the three low-index faces of platinum and rhodium in aqueous 0.1 M $HClO_4$ at 0 V vs NHE[67]. The lower spectra refer to saturated CO coverages and the companion upper spectra to a smaller coverage, θ_{CO}, as indicated. Several points can be gleaned from such results in comparison with corresponding uhv data. The proportion of CO bound in atop versus twofold bridging (or related) sites, as deduced from the ν_{CO} bands at ca 2000–2100 and 1800–1900 cm^{-1}, respectively, is seen to vary markedly with the crystallographic orientation. At least for saturated coverages on platinum, the site occupancies (and by inference the adlayer structures) are closely similar to those observed on the same surface in uhv. The ν_{CO} frequencies, however, are typically 20–30 cm^{-1} lower in the electrochemical environment. Greater behavioral differences between the electrochemical and uhv systems are discerned at lower CO coverages in that bridge bonding is much more prevalent in the former case. The latter may be ascribed to the effect of water (and in some cases hydrogen) coadsorption in the electrochemical systems[67].

A major part of these interesting spectral differences, however, can be understood in terms of the role of the electrochemical double layer in modifying

the surface potential across the CO adlayer. This point becomes apparent when the CO infrared spectral properties observed in corresponding electrochemical and uhv environments are compared on a common surface-potential scale. Although somewhat controversial[70], the so-called "absolute" potential of the normal hydrogen electrode (NHE), $E_k(ref)$, is about 4.6 (± 0.25) V. This allows the surface potential, ϕ_s^M, to be extracted from the electrode potential E (measured vs NHE or other convenient reference electrodes) by using[71]

$$\phi_s^M = E - |E_k(ref)| - \chi_s \qquad (1)$$

where χ_s is the solution-vacuum surface potential (usually $|\chi_s| \leq 0.1$–0.2 V).

The ϕ_s^M values obtained in this fashion for the metal-solution interface can be compared directly with the surface potentials for the corresponding metal-vacuum interface, ϕ_v^M, extracted from work-function measurements[64b,67]. Such comparisons show that the accessible range of surface potentials ϕ_s^M for platinum and rhodium electrodes with CO adlayers, (i.e. where CO is stable towards electrooxidation in acidic aqueous electrolytes, ≤ 0.5 V vs NHE), is considerably (0.5–1.0 V) below the ϕ_v^M values for the corresponding metal/CO interfaces in vacuum[64b,67,72]. This implies that the electrochemical surface potentials are decreased substantially by the double-layer environment. These surface-potential contributions generally arise from excess electronic charge σ_M countered by double-layer ionic charges ["free-charge" potential drop $g_s^M(ion)$] along with oriented solvent dipoles ["dipolar" component $g^s(dip)$] and with any consequent alterations in the "surface electronic" (electron spillover) portion of the metal work function when the surface is contacted with solution, χ_s^M. A general relation between the surface potentials for a given metal-adlayer system in electrochemical and uhv environments is[71]

$$\phi_s^M - \phi_v^M = g_s^M(ion) - g^s(dip) + \delta\chi^M \qquad (2)$$

Variations in ϕ_s^M are necessarily induced externally by altering σ_M and hence

$g_s^M(ion)$.

By using suitable nonaqueous media, ϕ_s^M for the electrochemical CO adlayers can be increased up to the ϕ_v^M value for the corresponding metal/CO–uhv interface[72]. Interestingly, the ν_{CO} frequencies as well as CO binding site occupancies for saturated CO adlayers in the electrochemical and uhv environments become very similar under these conditions, implicating clearly the importance of the surface potential in modifying the CO adlayer properties[72]. Further, by examining the effects of altering the double-layer cation on the ν_{CO} – E behavior, the condition $\phi_s^M \approx \phi_v^M$ was found to correspond to $g_s^M(ion) = 0$ (i.e. the so-called potential of zero charge, where $\sigma_M = 0$), inferring that $[\delta\chi^M - g^S(dip)]$ is only small and rather solvent-insensitive ($\lesssim$ 0.2–0.3 V)[72a,b].

The various influences of the surface potential upon the CO adlayer structure are illustrated for the Rh(111)/CO system in Figure 9, which shows infrared spectra obtained for a sequence of electrode potentials (vs NHE, as indicated) in CO-saturated 0.1 M $NaClO_4$[64a,73]. At low potentials (< –0.2 V), CO is seen to be bound chiefly in bridging sites, whereas at higher potentials the adlayer structure is characterized instead by predominant atop binding. The increasing preference for multifold CO coordination towards lower surface potentials is also seen on some other surfaces[73,75]. Within the potential region where the CO adlayer structure remains essentially invariant, the ν_{CO} frequencies are seen to upshift noticeably with increasing potential: at the electrode potential corresponding to $\phi_s^M = \phi_v^M$ (ca 1.2 V vs NHE), the band frequencies as well as CO site occupancies in the electrochemical and uhv environments are essentially coincident. The real-space adlayer structures for the electrochemical Rh(111)/CO system were also characterized by in-situ STM combined with IRAS[64a]. Interestingly, the high-potential structure, (2 × 2) – 3CO (θ = 0.75) deduced in this fashion is closely similar to that extracted for

the corresponding uhv system by means of dynamical LEED and vibrational spectroscopy[76].

The origin of the significant ν_{CO} – E (and hence ν_{CO} – ϕ_s^M) dependencies (typically 20–50 cm^{-1} v^{-1}), together with similar observations for other adsorbates, has engendered much discussion[69,77]. The relative importance of electrostatic field (first-order Stark) effects and adsorbate–surface charge sharing to the ν_{CO} – E dependencies is somewhat controversial[77b,c]. Lambert, however, has pointed out that interpretations involving the latter MO treatments are ultimately equivalent to the descriptions couched in terms of dipole moment/electrostatic-field effects with proper consideration of metal–adsorbate interactions[77a]. Indeed, the potential-induced changes in CO site occupancy, as in Figure 9, can be rationalized in terms of adsorbate dipole–field effects as well as by an MO treatment[67,78].

An interesting general issue that arises in the context of double-layer effects upon adlayer structure and bonding is the possible involvement of (and distinction between) specific rather than non-specific effects of the solvent and the electrolyte ions. A simple, albeit not unique, definition of non-specific double-layer effects is those that are determined merely by the surface potential, rather than additionally by the chemical nature of the dipolar or charged species contributing to ϕ_s^M. A closely related definition utilizes the surface charge density σ_M rather than the potential. This alternative formulation offers the advantage of maintaining constant the surface–adsorbate interactions, while the former (constant electrode-potential condition) is more readily applied in practice. (The question of the appropriate electrical variable, σ_M or E, was debated some years ago by Parsons, Frumkin, and Damaskin in connection with electrochemical adsorption isotherms[79].) At least for experiments involving variations in the electrolyte nature at a fixed adlayer

coverage, however, the distinction between a constant E or σ_M condition is usually only a subtle one.

Evidence favoring a dominant role of such nonspecific double-layer effects has been obtained for CO adlayers under some conditions. As already noted, ν_{CO} - ϕ_s^M dependencies are typically found to be largely independent of the solvent medium[72]. A related observation concerns the progressive atop-bridging site conversion induced for a saturated CO adlayer on Ni(111) in uhv by various polar solvent overlayers[80]. The extent of site conversion, as deduced from the relative infrared band intensities, was seen to correlate in a common fashion with the measured changes in the surface potential, irrespective of the nature of the solvent. This latter example is, however, distinct from the usual electrochemical situation where changes in the surface potential ϕ_s^M are induced fundamentally by variations in σ_M and hence the free ionic contribution, g_s^M(ion)[Eq. (2)], rather than the solvent dipolar term g^s(dip). Novel evidence supporting the appropriate value of σ_M rather than ϕ_s^M (or E) as the electrical variable was obtained from the near-common ν_{CO} - σ_M, but not ν_{CO} - E, behavior observed for several chargeable high-nuclearity Pt carbonyl clusters in comparison with electrochemical Pt/CO adlayers in nonaqueous media[81].

As alluded to above, one might anticipate that the nature of the electrolyte ions would often exert a more specific influence on adlayer structure and bonding. An example of such an effect, again for saturated CO adlayers at platinum-nonaqueous interfaces, is observed in the presence of alkali-metal cations[72b,c]. Unlike the larger tetraalkylammonium cations, alkali metal ions induce sharp transitions at lower potentials from atop to multifold CO coordination, driven apparently by Lewis acid-base interactions. This effect is analogous to cation-induced coordination shifts observed in polynuclear carbonyl complexes[72c].

While CO adlayers represent an optimal case for examining the effect of the double-layer environment upon adsorbate bonding, several other systems have been examined in this regard by vibrational spectroscopy, including thiocyanate and cyanide on platinum[83]. The effect of the electrical variable upon the metal surface-adsorbate bond is of particular fundamental interest. The low frequencies (and absorbances) of such vibrations largely preclude their examination by in-situ IRAS, although this situation may change with the advent of synchrotron infrared sources.

Nevertheless, SERS provides a sensitive means of extracting such ν_{M-X} - E data. A simple example of such applications of relevance to the above discussion concerns adsorbed halide adlayers on gold in aqueous media which yield metal-halide vibrations in the range of 120-300 cm^{-1}[85]. The ν_{M-X} - E slopes were found to decrease in the sequence $Cl^- > Br^- > I^-$, and vibrational force constants that tend to increase from Cl^- to I^-. These findings are consistent with an increasing extent of bond covalency from Cl^- to I^-[84], as also anticipated from electrosorption valency data[85]. As mentioned above, iodide adsorption on gold involves largely complete adsorbate-metal charge transfer. The contribution to the first-order Stark effect (and hence the positive ν_{M-X} - E slope) from the adsorbate charge-metal image dipole is therefore expected to be only minimal for adsorbed iodide (effectively adsorbed iodine atoms), accounting for the minimal ν_{M-X} - E dependence in this case. There appears to be considerable scope for more detailed applications of vibrational spectroscopy for the elucidation of such interfacial field effects upon adsorbate bonding.

CONCLUDING REMARKS

Along with the complementary insight provided by vacuum-based approaches, the emergence of increasingly diverse as well as powerful in-situ methods for

exploring the atomic- and molecular-level nature of metal-solution interfaces is clearly exerting a profound impact on the development of electrochemical surface science. The availability of the externally controlled electrical variable for in-situ studies, together with the multidimensional experimental picture afforded by coupling potential-dependent microscopic-level measurements with conventional electrochemical data, is clearly refashioning and even revolutionizing our appreciation of atomic-level phenomena in surface electrochemistry. The ramifications for fundamental electrochemistry are diverse. While largely structural in nature, it is hoped that the detailed information now obtainable on the atomic-/molecular-level properties of electrochemical interfaces will impact increasingly on our understanding of surface kinetic processes of practical as well as fundamental significance, such as electrocatalysis, corrosion, and electrodeposition.

Perhaps the most significant anticipated consequence of these experimental developments, however, is the emergence of a real commonality of understanding (and mutual appreciation) in electrochemical and vacuum-based surface science. While electrochemical systems often appear frighteningly, even hopelessly, complex to practioners in the latter area (especially to physicists!), they now offer some enticing opportunities for the exploration of microscopic-level interfacial phenomena of significance to surface science as a whole. These derive not only from the availability of the externally controllable electrical variable, but also from the intrinsically close link between catalytic chemistry and electrochemical systems, especially involving redox (and photochemical redox) processes. There is good reason, then, to anticipate that the development of a more unified experimental, and accompanying theoretical, understanding in these formerly disparate branches of surface chemistry is as inevitable as it is desirable.

Acknowledgements

We are grateful to Andy Gewirth, Joe Gordon, Alexei Kornyshev, Owen Melroy, Ben Ocko, and Mike Toney for sharing unpublished results and ideas. Antoinette Hamelin inspired us, as well as collaborated, in our microscopic endeavors. Several Weaver group members, especially Si Chang, Greg Edens, Ping Gao and Lam Leung, have also contributed importantly to our activities in this area. Finally, the continuing research support to MJW provided by the National Science Foundation and the Office of Naval Research is most gratefully acknowledged.

References

(1) Weaver, M.J., 1987. "Comprehensive Chemical Kinetics", Vol. 27, ed. R.G. Compton, Elsevier, Amsterdam, Chapter 1.

(2) Weaver, M.J., 1992. Chem. Revs. 92:463.

(3) Delahay. P., 1965. "Double Layer and Electrode Processes", Wiley-Interscience, New York.

(4) For example: Somorjai, G.A., 1981. "Chemistry in Two Dimensions - Surfaces", Cornell University Press, Ithaca.

(5) (a) Shannon, C., Frank, D.G., Hubbard, A.T., 1991. Ann. Rev. Phys. Chem., 42:393; (b) Hubbard, A.T., 1988. Chem. Revs. 88:633.

(6) Parsons, R. 1989. "Comprehensive Chemical Kinetics", Vol. 29, eds. R.G. Compton, A. Hamnett, Elsevier, Amsterdam, Chapter 3.

(7) Stuve, E., Kizhakevariam, N., 1993. J. Vac. Sci. Tech. A, in press.

(8) Sass, J.K., Bange, K., 1988. ACS Symp. Ser., 378:54.

(9) Wagner, F.T., 1993. "Frontiers in Electrochemistry", Vol. 2, eds. J. Lipkowcki, P.N. Ross, Jr., VCH Publishers, New York.

(10) (a) Clavilier, J., Faure, R., Guinet, G., Durand, R., 1980. J. Electroanal. Chem., 107:205; (b) Clavilier, J., 1980. J. Electroanal. Chem., 107:211.

(11) Clavilier, J., ACS Symp. Ser. 1988. 378:202.

(12) Zurawski, D., Rice, L., Hourani, M., Wieckowski, A., 1987. J. Electroanal. Chem., 230:221.

(13) Hamelin, A., 1986. "Modern Aspects of Electrochemistry", Vol. 16, Eds. B.E. Conway, R.E. White, J.O'M. Bockris, Plenum, New York, Chapter 1.

(14) (a) Wagner, F.T., Ross, P.N., Jr., 1988. J. Electroanal. Chem., 250:301; (b) Ross, P.N., Jr., 1988. ACS Symp. Ser. 378, 37.

(15) Bewick, A., Pons, S., 1985. "Advances in Infrared and Raman Spectroscopy", Eds. R.J.H. Clark, R.E. Hester, Wiley, New York, Vol. 12, Chapter 1.

(16) Binnig, G., Rohrer, H., 1987. Rev. Mod. Phys., 59:615.

(17) (a) Ogletree, F., Salmeron, M., 1990. Prog. Solid State Chem., 20:235; (b) Behm, R.J., Garcia, N., Rohrer, H., eds., 1990. "Scanning Tunneling Microscopy and Related Methods", Kluwer Publishers, Dordrecht; (c) Chen, C.J., 1993. "Introduction to Scanning Tunneling Microscopy", Oxford University Press, U.K.

(18) Magnussen, O.M., Hotlos, J., Nichols, R.J., Kolb, D.M., Behm, R.J., 1990. Phys. Rev. Lett., 64:2929.

(19) Yau, S-L., Vitus, C.M., Schardt, B.C., 1990. J. Am. Chem. Soc., 112:3677.

(20) Gao, X., Zhang, Y., Weaver, M.J., 1992. J. Phys. Chem., 96:4156.

(21) (a) Toney, M.F., Melroy, O.R., 1991. "Electrochemical Interfaces: Modern Techniques for In-Situ Interface Characterization", ed. H.D. Abruña, VCH Publishers, New York, Chapter 2; (b) Abruña, H.D., 1991. Chapter 1 in ref. 21a.

(22) (a) Ross, P.N., Jr., 1993. Ref. 9, Chapter ___; (b) Kolb, D.M., 1993. Ref. 9, Chapter 3.

(23) Hamelin, A., 1982. J. Electroanal. Chem., 142:299.

(24) For example: Van Hove, M.A., Wang, S-W., Ogletree, D.F., Somorjai, G.A., 1989. Adv. Quantum Chem., 20:1.

(25) (a) Schneider, J., Kolb, D.M., 1988. Surf. Sci., 193:579; (b) Kolb, D.M., Schneider, J., 1986. Electrochim. Acta, 31:929; (c) Kolb, D.M., Schneider, J., 1985. Surf. Sci., 162:764; (d) Zei, D.M., Lehmpfuhl, G., Kolb, D.M., 1989. Surf. Sci., 221:23.

(26) Friedrich, A., Pettinger, B., Kolb, D., Lüpke, G., Steinhoff, R., Marowsky, G., 1987. 123

(27) Pettinger, B., Lipkowski, J., Mirwald, S., Friedrich, A., 1992. J. Electroanal. Chem., 329:289.

(28) (a) Ocko, B.M., Wang, J., Davenport, A., Isaacs, H., 1990. Phys. Rev. Lett., 65:1466; (b) Tidswell, I.M., Markovic, N.M., Lucas, C.A., Ross, P.N., 1993. Phys. Rev. B, in press.

(29) Wang, J., Ocko, B.M., Davenport, A.J., Isaacs, H.S., 1992. Phys. Rev. B, 46:10321.

(30) Ocko, B.M., Helgensen, G., Schardt, B., Wang, J., Hamelin, A., 1992. Phys. Rev. Lett., 69:3350.

(31) Gao, X., Hamelin, A., Weaver, M.J., 1991. J. Chem. Phys., 95:6993.

(32) (a) Gao, X., Hamelin, A., Weaver, M.J., 1991. Phys. Rev. Lett., 67:618; (b) Gao, X., Hamelin, A., Weaver, M.J., 1992. Phys. Rev. B, 46:7096; (c) Hamelin, A., Gao, X., Weaver, M.J., 1992. J. Electroanal. Chem., 323:361; (d) Gao, X., Edens, G., Hamelin, A., Weaver, M.J., in preparation.

(33) Gao, X., Hamelin, A., Weaver, M.J., 1991. Phys. Rev. B, 44:10983.

(34) (a) Gao, X., Hamelin, A., Weaver, M.J., 1992. Surf. Sci., 274:L588; (b) Gao, X., Hamelin, A., Weaver, M.J., in preparation.

(35) (a) Tao, N.J., Lindsay, S.M., 1991. J. Appl. Phys., 70:5141; (b) Tao, N.J., Lindsay, S.M., 1992. Surf. Sci., 274:L546.

(36) Hotlos, J., Magnusson, O.M., Behm, R.J., Batina, N., Kolb, D.M., to be published.

(37) Magnusson, O.M., Wiechers, J., Behm, R.J., 1993. Surf. Sci., in press.

(38) Liew, Y-F., Wang, G-C., 1990. Surf. Sci., 227:190.

(39) Ross, P.N., D'Agostino, A.T., 1992. Electrochim. Acta, 37:615.

(40) Korneyshev, A.A., Vilfan, I., 1993. Phys. Rev. B, in press.

(41) Wintterlin, J., Behm, R.J., 1992. "Scanning Tunneling Microscopy I," Springer Series in Surface Sciences, Vol. 20, ed. H-J. Güntherodt, R. Wiesdanger, Springer-verlag, Berlin and Heidelberg, Chapter 4.

(42) Schardt, B.C., Yau, S-L., Rinaldi, F., 1989. Science, 243:150.

(43) Gao, X., Weaver, M.J., 1992. J. Am. Chem. Soc., 114:8544.

(44) Gao, X., Weaver, M.J., 1993. Ber. Bunsenge. Phys. Chem., in press.

(45) Gao, X., Edens, G., Weaver, M.J., in preparation.

(46) Ocko, B.M., et al to be published.

(47) Bravo, B.G., Michelbaugh, S.L., Soriaga, M.P., Villegas, I., Suggs, D.W., Stickney, J.L., 1991. J. Phys. Chem., 95:5245.

(48) (a) Haiss, W., Sass, J.K., Gao, X., Weaver, M.J., 1992. Surf. Sci., 274:L593; (b) Haiss, W., Gao, X., additional unpublished results.

(49) For example: Valette, G., Hamelin, A., Parsons, R., 1978. Z. Physik. Chem., N.F., 113:71.

(50) Nguyen Van Huong, C., Hinnen, C., Rousseau, A., 1983. J. Electroanal. Chem., 151:149.

(51) Tao, N.J., Lindsay, S.M., 1992. J. Phys. Chem., 96:5213.

(52) Gao, X., Weaver, M.J., to be published.

(53) Magnussen, O.M., Hageböck, J., Hotlos, J., Behm, R.J., 1993. Disc. Far. Soc., in press.

(54) (a) Toney, M.F., et al, 1992. Phys. Rev. B., 45:9362; (b) Toney, M.F., et al, 1990. Phys. Rev. B, 42:5594; (c) Toney, M.F., et al, 1993. J. Electrochem. Soc., in press; (d) Melroy, O.R., et al, 1988. Phys. Rev. B, 38:10962; (e) Melroy, O.R., et al, 1989. J. Electroanal. Chem., 258:403; (f) Toney, M.F., et al, 1991. Langmuir, 7:796; (g) Toney, M.F., et al, 1991. Proc. SPIE Vol. 1550:140.

(55) (a) Manne, S., Hansma, P.K., Massic, J., Elings, V.B., Gewirth, A.A., 1991. Science, 251:183; (b) Chen, C-H., Vesecky, S.M., Gewirth, A.A., 1992. J. Am. Chem. Soc., 114:451; (c) Chen, C-C., Gewirth, A.A., 1992. Phys. Rev. Lett., 68:1571; (d) Chen, C-H., Gewirth, A.A., 1992. J. Am. Chem. Soc., 114:5439.

(56) Chen, C-H., Kepler, K.D., Gewirth, A.A., Wang, J., Ocko, B.M., 1993. J. Phys. Chem., in press.

(57) (a) Haiss, W., Lackey, D., Sass, J.K., Meyer, H., Nichols, R.J., 1992. Chem. Phys. Lett., 200:343; (b) Batina, N., Will, T., Kolb, D.M., 1993. Disc. Far. Soc., in press.

(58) (a) Hachiya, T., Honbro, H., Itaya, K., 1991. J. Electroanal. Chem., 315:275; (b) Sashikata, K., Furuya, N., Itaya, K., 1991. J. Electroanal. Chem., 316:361.

(59) For example: Kolb, D.M., 1984. "Advances in Electrochemistry and Electrochemical Engineering:, eds. H. Gerischer, C. Tobias, Vol. 11, Wiley, New York, p. 125.

(60) (a) Lynch, M.L., Barner, B.J., Corn, R.M., 1991. J. Electroanal. Chem., 300:447; (b) Lynch, M.L., Corn, R.M., 1990. J. Phys. Chem., 94:4382.

(61) Gao, X., Zhang, Y., Weaver, M.J., 1992. J. Phys. Chem., 96:4156.

(62) For example: (a) Tao, N.J., Pan, J., Li, Y., Oden, P.I., DeRose, J.A., Lindsay, S.M., 1992. Surf. Sci., 271:L338; (b) Green, M.P., Hanson, K.J., Carr, R., Lindau, I., 1990. J. Electrochem. Soc., 137:3493.

(63) Tao, N.J., DeRose, J.A., Lindsay, S.M., 1993. J. Phys. Chem., 97:910.

(64) (a) Yau, S-L., Gao, X., Chang, S-C., Schardt, B.C., Weaver, M.J., 1991. J. Am. Chem. Soc., 113:6049; (b) Gao, X., Chang, S-C., Jiang, X., Hamelin, A., Weaver, M.J., 1992. J. Vac. Sci. Tech. A, 10:2972.

(65) Recent reviews on electrochemical IRAS include:(a) Christensen, P., Hamnett, A., 1989. "Comprehensive Chemical Kinetics", Vol. 29, eds. R.G. Compton, A. Hamnett, Chapter 2; (b) Nichols, R.J., 1992. "Adsorption of Molecules at Metal Electrodes", Frontier of Electrochemistry Vol. 1, eds. J. Lipkowski, P.N. Poss, VCH Publishers, New York, Chapter 7; (c) Stole, S.M., Popenoe, D.D., Porter, M.D., 1991. "Electrochemical Interfaces", Ed. H.D. Abruña, VCH Publishers, New York, Chapter 7.

(66) Recent reviews on electrochemical SERS include: (a) Weitz, D.A., Moskovits, M., Creighton, J.A., 1986. In "Chemistsry and Structure at Interfaces - New Laser and Optical Techniques", eds. R.B. Hall, A.G. Ellis, VCH Publishers, Deerfield Beach, FL, Chapter 5; (b) Hester, R.E., 1989. In "Comprehensive Chemical Kinetics", eds. R.G. Compton, A. Hamnett, Elsevier, Amsterdam, Vol. 29, Chapter 2; (c) Pettinger, B., as ref. 65c, Chapter 6; (d) Pemberton, J.E., as ref. 65d, Chapter 5.

(67) Chang, S-C., Weaver, M.J., 1991. J. Phys. Chem., 95:5391.

(68) Parsons, R. Vandernoot, T., 1998. J. Electroanal. Chem., 257:9.

(69) Weaver, M.J., 1993. App. Surf. Sci., in press.

(70) For example: Hansen, W.N., Hansen, G.J., 1988. ACS Symp. Ser., 378:166.

(71) Trasatti, S., 1983. J. Electroanal. Chem., 150:1.

(72) (a) Chang, S-C., Jiang, X., Roth, J.D., Weaver, M.J., 1991. J. Phys. Chem., 95:5378; (b) Jiang, X., Weaver, M.J., 1992. Surf. Sci., 275:237; (c) Roth, J.D., Weaver, M.J., 1992. Langmuir, 8:1451.

(73) Chang, S-C., Weaver, M.J., 1990. Surf. Sci., 238:142.

(74) For example: Leung, L-W.H., Weaver, M.J., 1987. J. Am. Chem. Soc. 109:5113.

(75) Kitamura, F., Takahashi, M., Ito, M., 1988. J. Phys. Chem., 92:3320.

(76) Van Hove, M.A., Koestner, R.J., Frost, J.C., Somorjai, G.A., 1983. Surf. Sci., 129:482.

(77) For example: (a) Lambert, D.K., 1988. J. Chem. Phys., 89:3847; (b) Anderson, A.B., 1990. J. Electroanal. Chem., 280:37; (c) Bagus, P.S., Pacchioni, G., 1990. Surf. Sci., 236:233; (d) Korzeniewski, C., Pons, S., Schmidt, P., Severson, M.W., 1986. J. Chem. Phys., 85:4153.

(78) Chang, S-C., Weaver, M.J., 1993. J. Phys. Chem., in press.

(79) (a) Parsons, R., 1963. J. Electroanal. Chem., 7:136; 8:93; (b) Frumkin, A.N., 1963. J. Electroanal. Chem., 7:152; (c) Damaskin, B.B., 1963. J. Electroanal. Chem., 7:155.

(80) Xu, Z., Yates, J.T., Wang, L.C., Kreuzer, H.J., 1992. J. Chem. Phys., 96:1628.

(81) Roth, J.D., Lewis, G.J., Safford, L.K., Jiang, X., Dahl, L.F., Weaver, M.J., 1992. J. Am. Chem. Soc., 114:6159.

(82) Ashley, K., Samant, M.G., Seki, H., Philpott, M.R., 1989. J. Electroanal. Chem., 270:349.

(83) (a) Rosasco, S.D., et al, 1985. J. Electroanal. Chem., 188:95; (b) Paulissen, V.B., Korzeniewski, C., 1992. J. Phys. Chem., 96:4563.

(84) Gao, P., Weaver, M.J., 1986. J. Phys. Chem., 90:4057.

(85) Deakin, M.R., Li, T-T., Melroy, O., 1988. J. Electroanal. Chem., 243:343.

FIGURE CAPTIONS

Fig. 1

Height-shaded atomic-resolution STM image of Au(100) at −0.3 V vs SCE in 0.1 M $HClO_4$, showing emergence of (5 × 27) reconstruction (left-hand side) and adjoining (1 × 1) domain (from ref. 32b).

Fig. 2

STM images obtained for Au(100) in 0.1 M H_2SO_4 during positive-going 10 mV s^{-1} sweep. A and B were obtained while electrode potential was swept from 0.1 to 0.3 V and 0.3 to 0.5 V, respectively (see text). [X. Gao, unpublished results.]

Fig. 3

Cyclic voltammogram at 50 mV s^{-1} obtained for ordered Au(111) in aqueous 0.1 M $NaClO_4$ + 5 mM NaI. [G. Edens, unpublished results.]

Fig. 4

STM image of atomic iodine adlayers on Au(111) in 0.1 M $HClO_4$ + 0.5 mM KI. A) "Composite-domain" image, showing (1 × 1) substrate (lower portion) and approximate (5 × $\sqrt{3}$) adlayer (upper portion), formed by stepping from −0.4 to 0.1 V vs SCE during data acquisition. B) Noncommensurate compressed iodine adlayer, at 0.25 V vs SCE (from ref. 43).

Fig. 5

Schematic simplified summary of iodine coverage-electrode potential relations on Au(111) and Au(110) with associated structures as determined by in-situ STM and GIXS. (Region I in both cases refers to low-coverage disordered adlayer, with coverages extracted from capacitance-potential measurements. Data on Au(110) are omitted at higher coverages due to the occurrence of slow phase transitions.)

Fig. 6

A) Ball-model structure of upd Bi on Ag(111) in 0.1 M $HClO_4$ as determined by GIXS. The Bi layer is commensurate ($\sqrt{3}$) in the a direction, but noncommensurate in the b direction. B) Dependence of upd Bi lattice constants in a and b direction upon electrode potential (vs Ag/AgCl), in absence (filled circles) and presence (open circles) of 0.35 mM Cl^- (from ref. 54g).

Fig. 7

In-situ AFM images (5 × 5 nm) of upd Bi on Au(111) in 0.1 M $HClO_4$. A) Image of (1 × 1) substrate. B) Image of (2 × 2) Bi adlayer (θ = 0.25), obtained at potentials just negative of upd peaks. C) Image of uniaxially commensurate high-coverage upd Bi structure (cf Fig. 6A), obtained at more negative potentials. D) Ball models of above structures (from ref. 55d).

Fig. 8

Representative infrared spectra (on common absorbance scale) for CO adlayers on platinum and rhodium low-index surfaces at 0 V vs NHE in aqueous 0.1 M $HClO_4$ (from ref. 67).

Fig. 9

Potential-dependent sequence of infrared spectra for CO adlayer on Rh(111) in CO-saturated 0.1 M $NaClO_4$. Potentials indicated are versus NHE (from ref. 74).

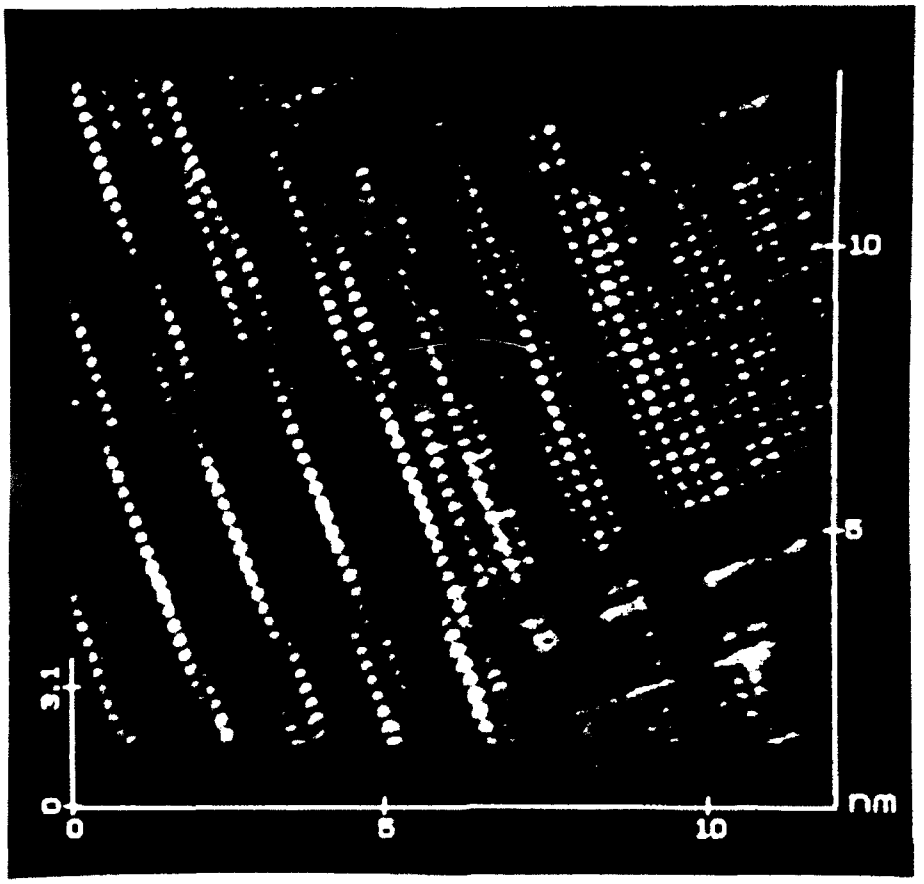

Fig.1

A

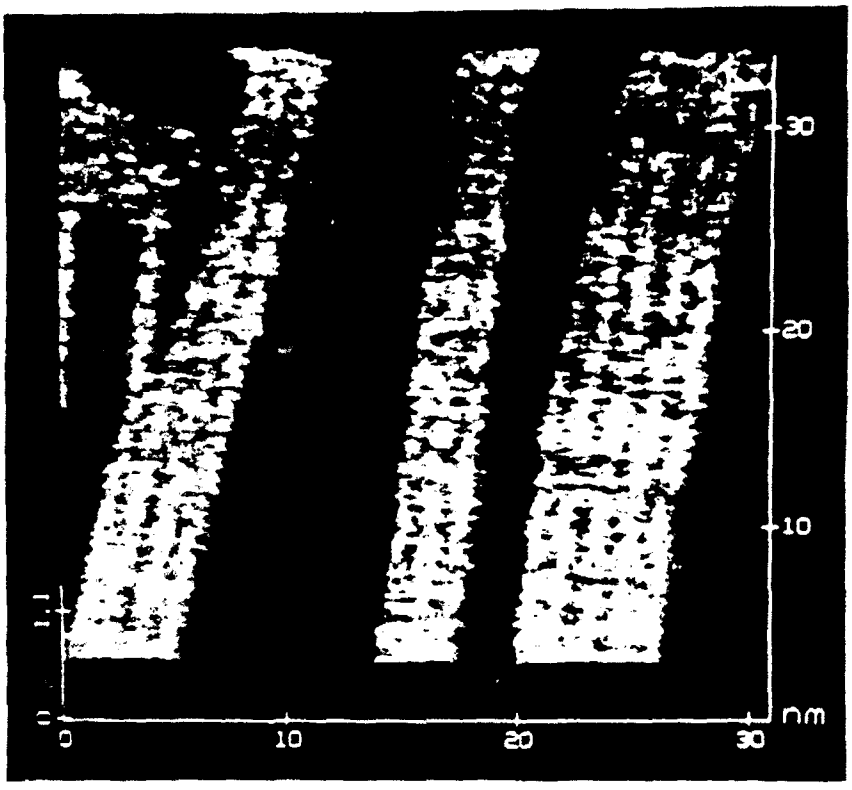

B

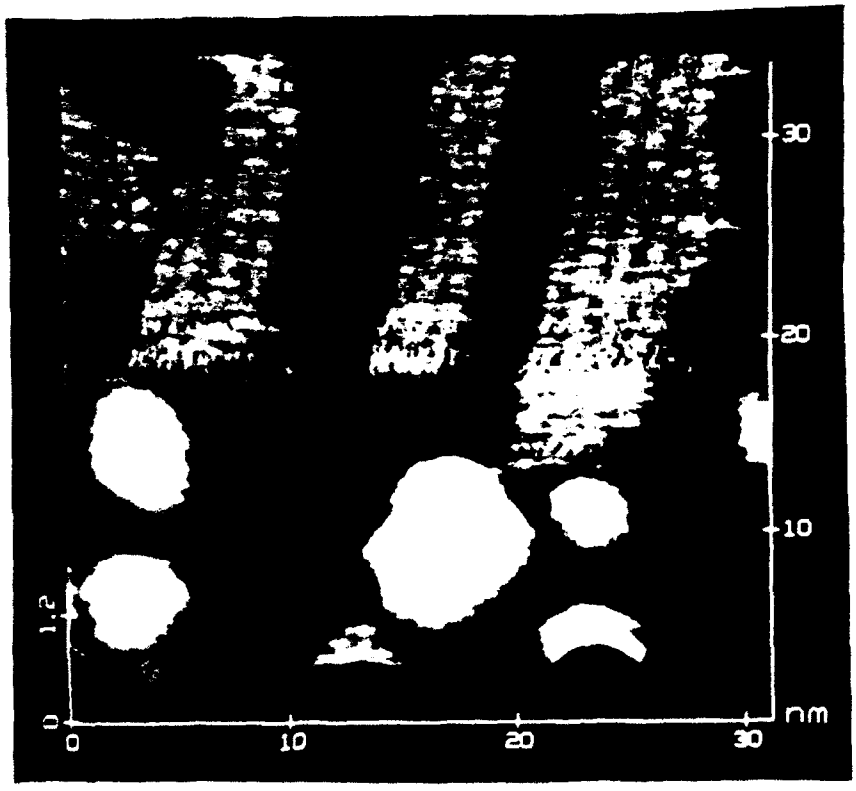

Fig.2

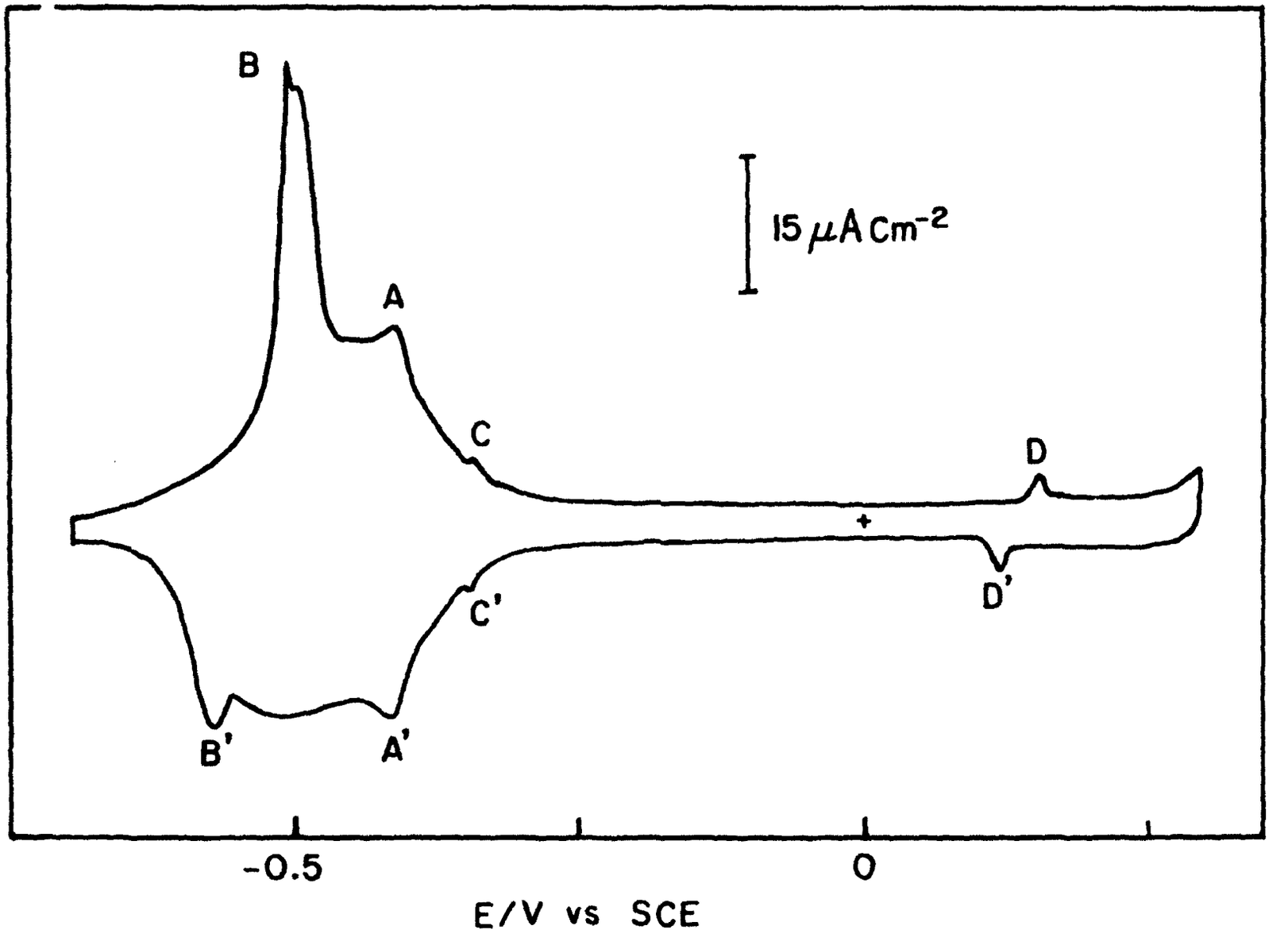

Fig.3

A

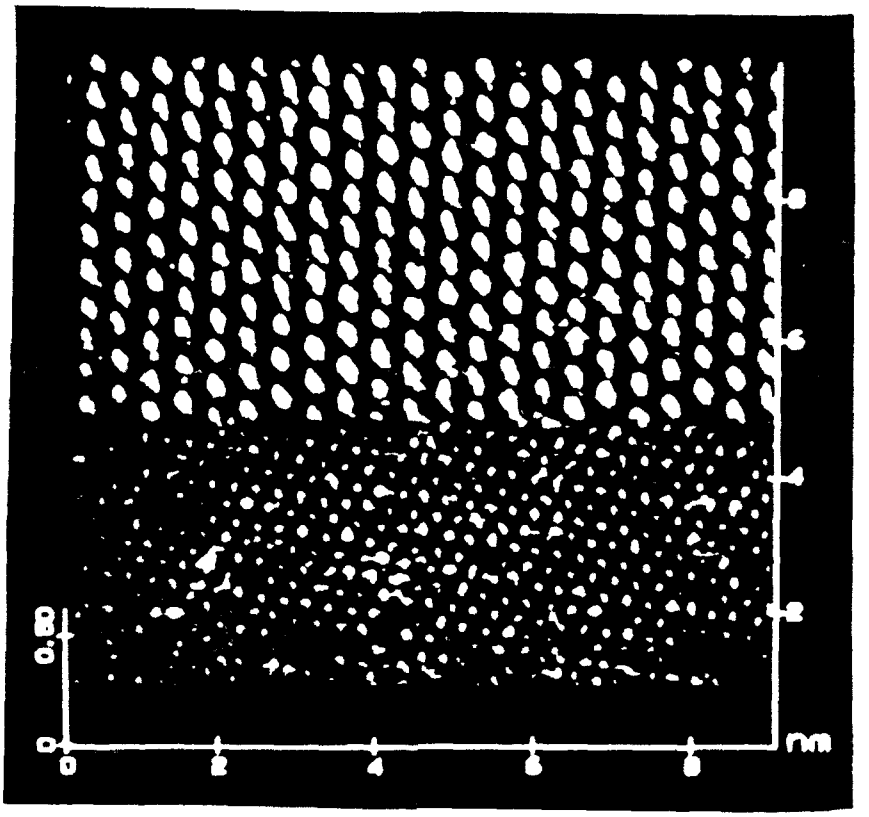

B

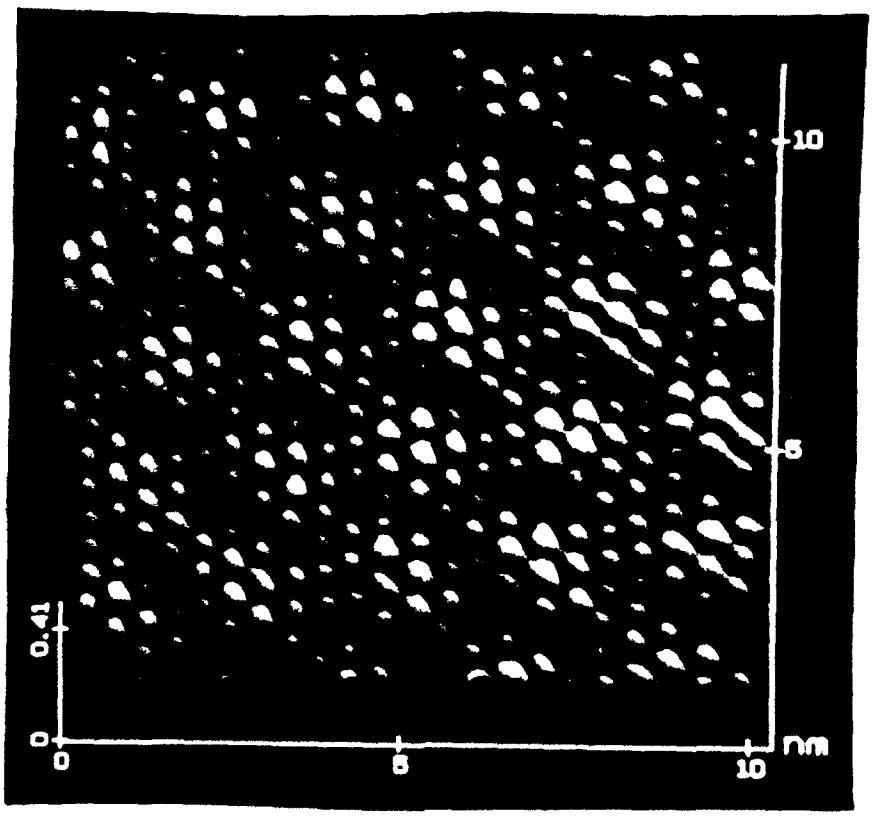

Fig.4

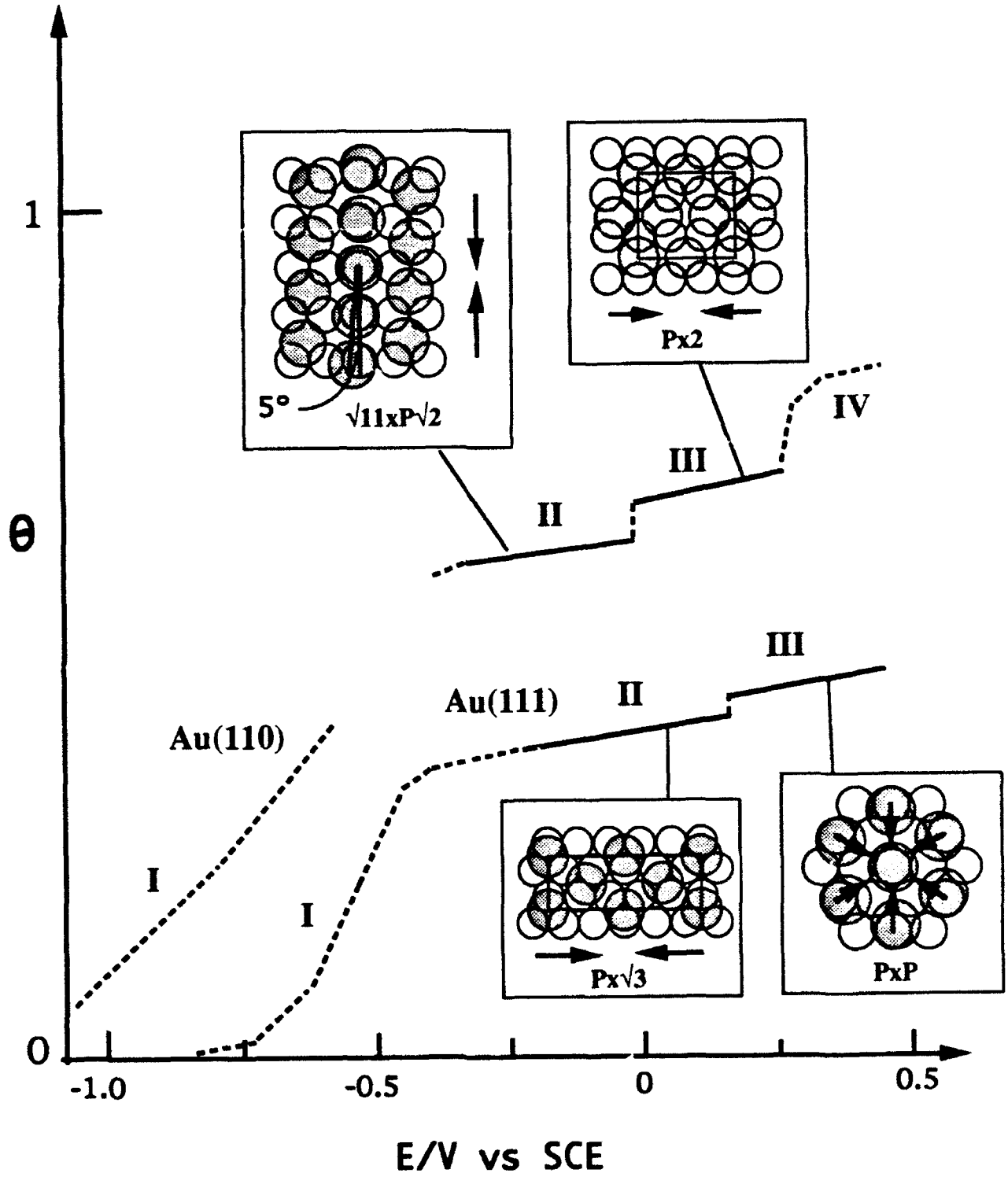
1
θ
0
5°
√11xP√2
Px2
IV
III
II
III
Au(111)
II
Au(110)
I
I
Px√3
PxP
-1.0
-0.5
0
0.5
E/V vs SCE

Fig.5

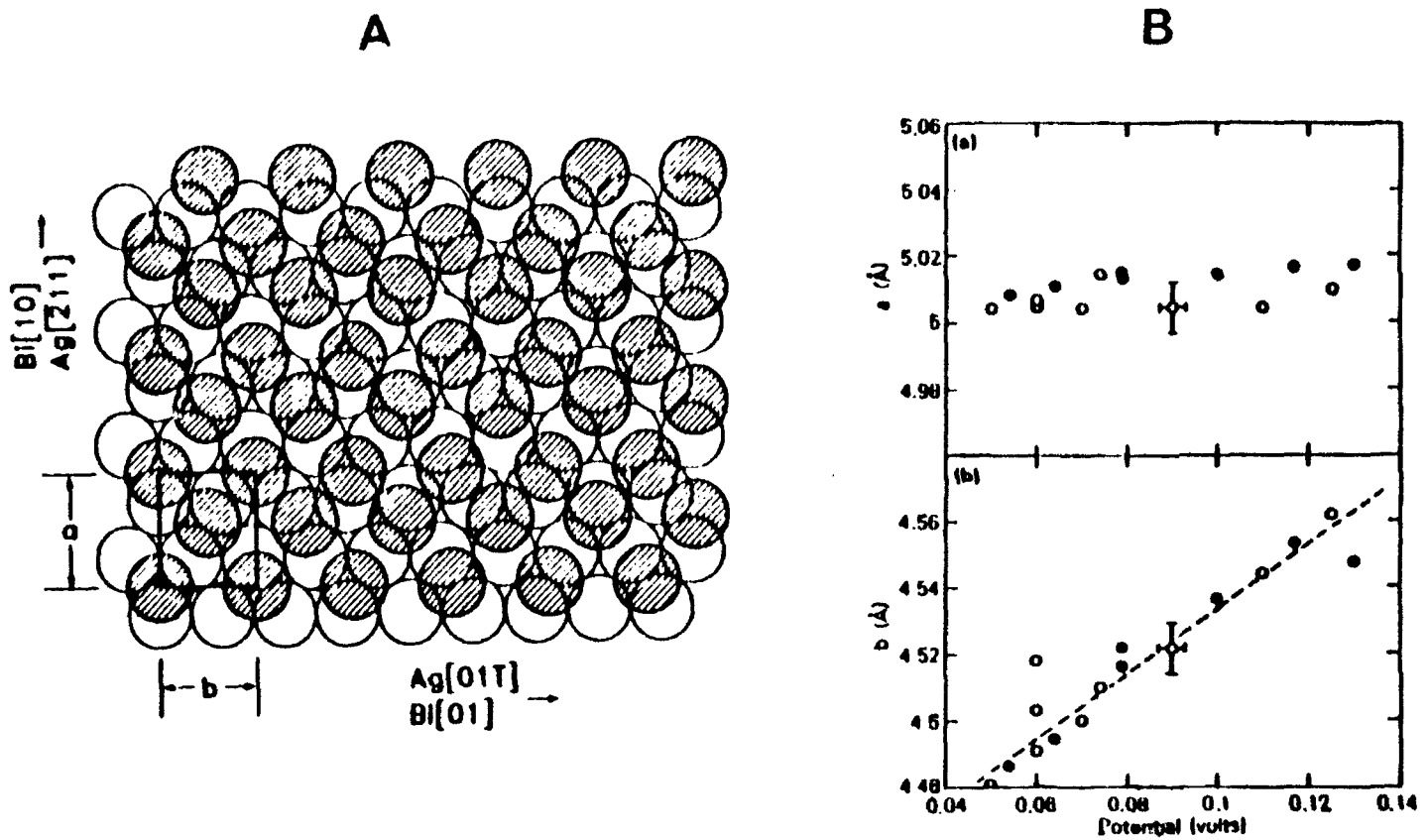
A
B
Bi[10]
Ag[2T1]
a
b
Ag[01T]
Bi[01]
(a)
(b)
a (Å)
b (Å)
5.06
5.04
5.02
5
4.98
4.56
4.54
4.52
4.5
4.48
0.04
0.06
0.08
0.1
0.12
0.14
Potential (volts)

Fig.6

Bi Monolayers on Au(111)

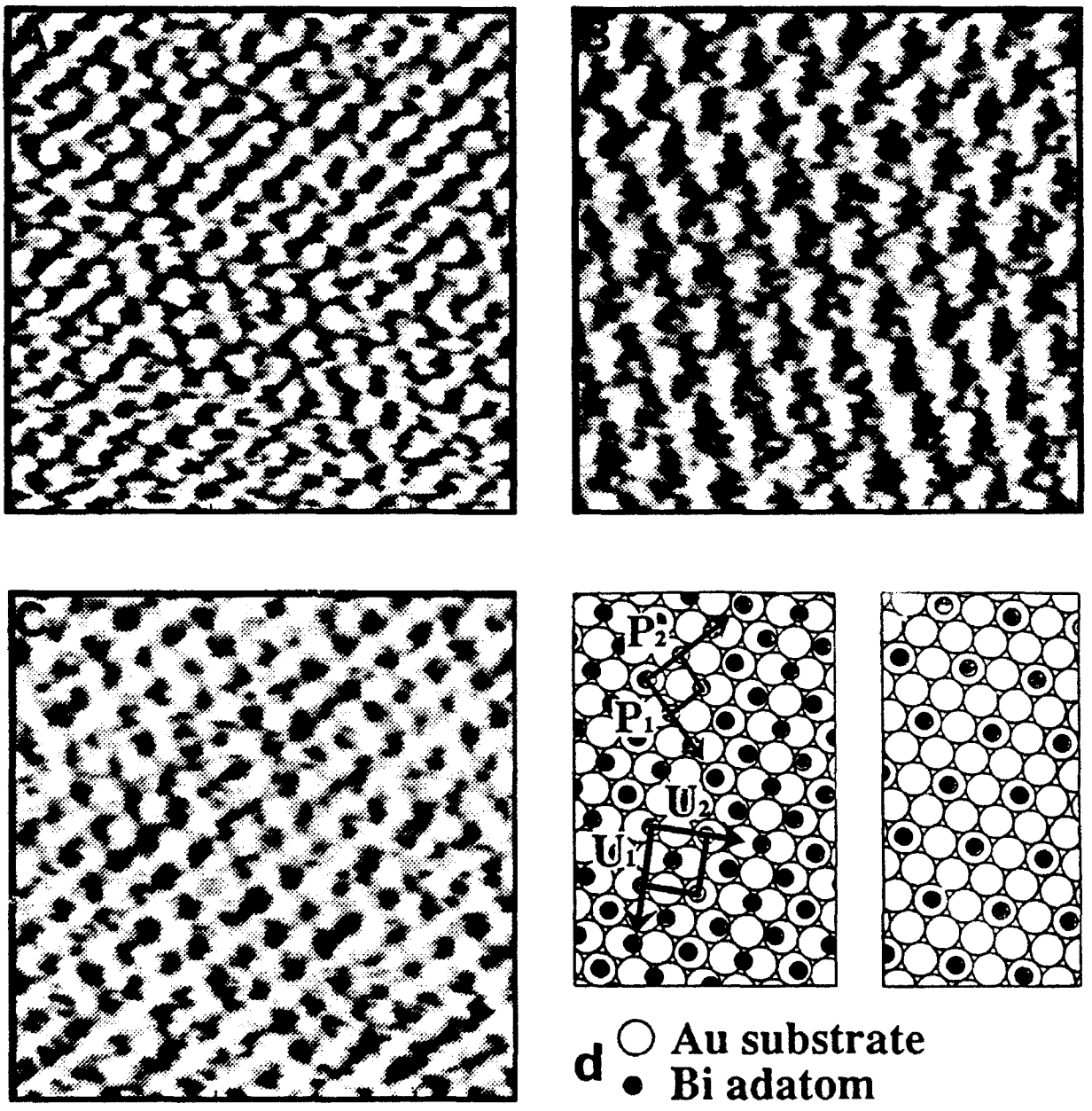

Fig. 7

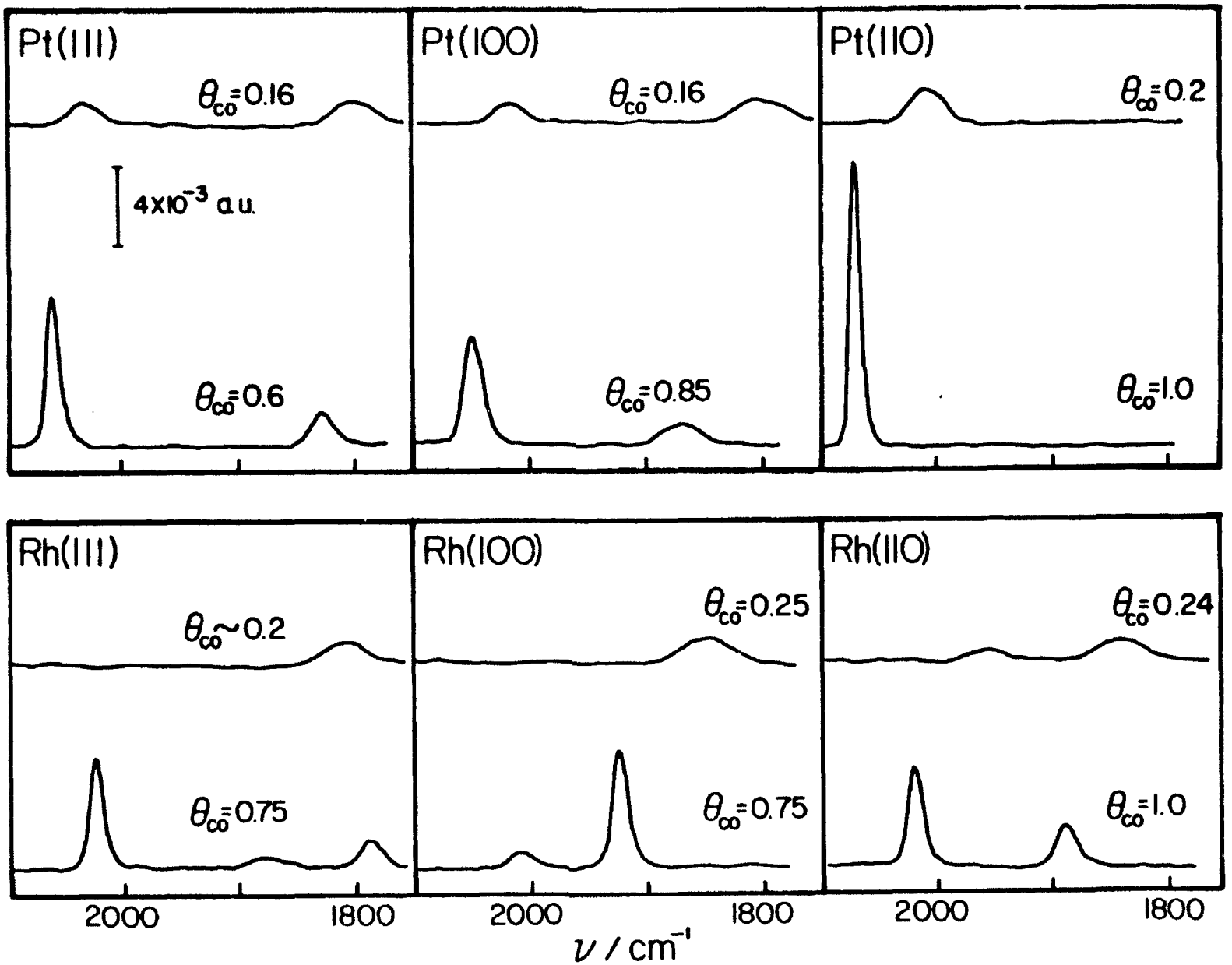
Pt(111)
θ_{CO}=0.16
4x10^{-3} a.u.
θ_{CO}=0.6
Pt(100)
θ_{CO}=0.16
θ_{CO}=0.85
Pt(110)
θ_{CO}=0.2
θ_{CO}=1.0
Rh(111)
θ_{CO}~0.2
θ_{CO}=0.75
Rh(100)
θ_{CO}=0.25
θ_{CO}=0.75
Rh(110)
θ_{CO}=0.24
θ_{CO}=1.0
2000
1800
2000
1800
2000
1800
ν / cm^{-1}

Fig.8

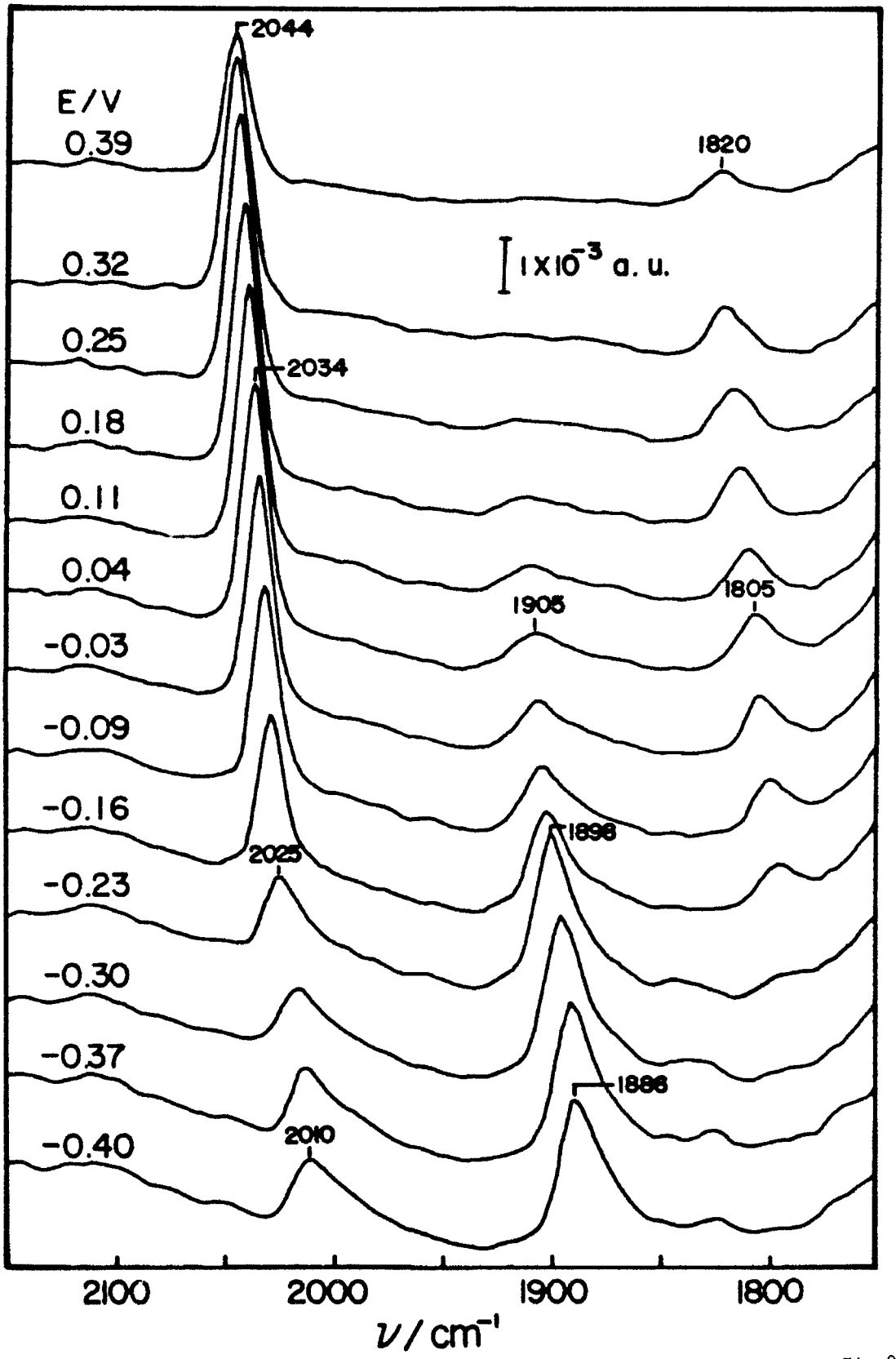
2044
E/V
0.39
1820
0.32
1×10⁻³ a. u.
0.25
2034
0.18
0.11
0.04
1805
1905
-0.03
-0.09
-0.16
1898
2025
-0.23
-0.30
-0.37
1886
2010
-0.40
2100
2000
1900
1800
ν / cm⁻¹

Fig.9